THE ROLE OF METFORMIN ON NON-SMALL CELL LUNG CANCER PROGRESSION
AND SKELETAL MUSCLE HEALTH

by

Nicole Lynn-Stott Bond

A dissertation submitted to the faculty of
The University of North Carolina at Charlotte
in partial fulfillment of the requirements
for the degree of Doctor of Philosophy in
Biology

Charlotte

2021

Approved by:

_____
Dr. Joseph Marino

_____
Dr. Michael Turner

_____
Dr. Didier Dréau

_____
Dr. Ian Marriott

_____
Dr. Jeanette Bennett

ABSTRACT

NICOLE LYNN-STOTT BOND. The Role of Metformin on Non-Small Cell Lung Cancer Progression and Skeletal Muscle Health. (Under the direction of Dr. JOSEPH MARINO)

Lung cancer is the second most common cancer and maintains a relatively small survival rate (~20%). Non-Small Cell Lung Cancer (NSCLC) makes up 80-85% of all lung cancer diagnoses. Lung cancer patients routinely undergo surgical procedures, chemotherapy, and/or radiation and these therapies can drive ongoing systemic issues, greatly hindering patient welfare and recovery timelines. Importantly, chemotherapy and radiation can induce deleterious systemic side effects, particularly within skeletal muscle, that are not reversible even in remission. We conducted experiments to determine whether Metformin can reduce lung cancer tumor burden in immunocompetent mice while maintaining skeletal muscle health. C57BL/6 mice were given Lewis Lung Cancer (LL/2), a form of NSCLC, orthotopically into the left lung. The LL/2 cells contained a bioluminescent reporter to track tumor growth *in vivo* with an imaging system. Control animals received a vehicle treatment of 1x phosphate buffered saline and Metformin treated animals received a Metformin (250mg/kg) twice a week. Tumor growth was monitored over the duration of the study and analyses were conducted to assess the efficacy of Metformin as a tumor suppressor *in vivo* (Chapter 2). To determine whether Metformin supports skeletal muscle health in mice with NSCLC, skeletal muscle homogenates from the cancer-bearing mice were analyzed for changes in genes and proteins related to inflammation, muscle mass, and metabolism (Chapter 3). Several experiments were conducted with LL/2 cells *in vitro* to determine the mechanisms by which Metformin alters the oncogenic program of NSCLC (Chapter 4). Understanding mechanisms by which Metformin influences NSCLC progression

could lead to potential therapeutic options for enriched targeted therapy. Importantly, assessing how Metformin may support skeletal muscle health throughout lung cancer progression could contribute clinically meaningful improvements for cancer patients.

DEDICATION

To my parents, Mark and Shari, and my husband,
Tyson – this work is dedicated to you.

ACKNOWLEDGEMENTS

TABLE OF CONTENTS

LIST OF TABLES

LIST OF FIGURES

LIST OF ABBREVIATIONS

ADP   Adenosine diphosphate

AMP   Adenosine monophosphate

AMPK   5' Adenosine Monophosphate-Activated Protein Kinase

ATP   Adenosine triphosphate

cDNA   Complimentary Deoxyribose Nucleic Acid

CDK4   Cyclin Dependent Kinase 4

FOXO3a   Forkhead Box O3

GAPDH   Glyceraldehyde 3-Phosphate Dehydrogenase

HES1   Hairy and Enhancer of Split 1

IGF-IR   Insulin Like Growth Factor 1 Receptor

IL-6   Interleukin 6

I.P.   Intraperitoneal

IVIS   In Vitro Imaging System

LKB-1   Liver kinase B 1

LL/2   Lewis Lung Carcinoma Cells

MAFBx   Muscle RING finger 1 and muscle atrophy F-box

MAPK   Mitogen activated protein kinase

mRNA   Messenger Ribonucleic Acid

mTOR   Mammalian Target of Rapamycin

NAD   Nicotinamide adenine dinucleotide

NADH   Nicotinamide adenine dinucleotide with hydrogen

NCID   Notch intracellular domain

NFkB	Nuclear factor kappa-light-chain-enhancer of activated B cells
NSCLC	Non-Small Cell Lung Carcinoma
OCT	Organic Cation Transporter
PAGE	Polyacrylamide Gel Electrophoresis
PCR	Polymerase Chain Reaction
PBS	Phosphate Buffered Saline
PGC-1α	Peroxisome Proliferator-Activated Receptor-γ Coactivator 1 Alpha
PIP3	Phosphatidylinositol-3,4,5-triphosphate
PTEN	Phosphatase and Tensin Homolog
P21	Protein 21
P27	Protein 27
P53	Protein 53
qPCR	Real-time Polymerase Chain Reaction
REDD1	Regulated in development and DNA damage responses 1
RIPA	Radioimmunoprecipitation Assay
RNA	Ribonucleic Acid
SDS	Sodium Dodecyl Sulfate
SEER	Surveillance, Epidemiology, and End Results
pSTAT3	Phosphorylation on Signal Transducer and Activator of Transcription 3
STAT3	Signal Transducer and Activator of Transcription 3
TNF-α	Tumor Necrosis Factor Alpha
TSC1/2	Tumor sclerosis complex 1 and 2
WB	Western Blot

CHAPTER 1: PROPOSED RESEARCH

1.1 Background and Significance

Lung cancer is the second most common cancer in both males and females [2]. Lung cancer was responsible for ~1.8 million cancer-related deaths globally in 2018 (World Health Organization Database), and is projected to remain a top cancer diagnosis and a leading cause of death in the United States with a projection of 156,000 fatalities in 2030 [3]. Cigarette smoke has been one of the largest contributors to lung cancer diagnoses, but a combination of lifestyle, genetic, and environmental components can contribute to an individual's risk and development of lung cancer [4]. Of the two types of lung cancer diagnoses, Small Cell Lung Carcinoma and Non-Small Cell Lung Carcinoma (NSCLC), NSCLC makes up 80-85% of all new lung cancer diagnoses [4]. The prevalence of NSCLC diagnoses suggests an utmost need to continue finding measures to reduce lung cancer risk, decrease tumor progression, and combat the projected burden of diagnoses over the next decade.

When healthy tissues are exposed to carcinogens, radiation, viral infections, chronic inflammation, or genetic mutations, healthy cells can acquire oncogenes, resulting in transformed cells that can express tumor antigens, dysregulate proper cell cycle progression, and undergo abnormal cell growth [5, 6]. Cancer patients often undergo surgical procedures, chemotherapy, or radiation to reduce cancer progression, but these interventions can drive ongoing systemic issues, greatly hindering patient welfare and recovery timelines [7]. While these therapies are beneficial, they induce irreversible effects, particularly in skeletal muscle, the largest the largest insulin sensitive and metabolically active tissue in the body [8, 9].

More than 50% of lung cancer patients undergoing chemotherapy or radiotherapy or a combination of both develop cachexia, a multi-faceted condition that results in an ongoing loss

of adipose tissue and skeletal muscle [10-13]. Cancer-induced cachexia degrades intracellular skeletal muscle proteins and damages satellite cells leading to skeletal muscle atrophy and decreased quality of life [9, 14-16]. Moreover, cancer-induced cachexia can lead to 85% loss of these tissues, resulting in imbalanced protein synthesis, alterations in mitochondria, and functional impairment [9, 17]. Skeletal muscle loss is often associated with metabolic dysfunction and insulin resistance, leaving patients with perturbed systemic metabolism [8, 14]. The degree of cancer-induced cachexia is inversely correlated with survival time, irrespective of tumor mass or the presence of metastases [9, 16]. Cachexia induced effects are not easily reversible though nutritional support, making the repercussions even more debilitating [9, 15]. To combat these issues, continuous advances are ongoing to bring new insight into oncology therapeutics [18]. Repurposing drugs provides an attractive tactic to improve cancer therapies, especially since new drug characterization and approval requires extensive investment and time [19]. Observational studies, pre-clinical trials, and clinical trials have provided insight into the efficacy of drug repositioning both for cancer prevention and cancer therapy [20]. Metformin, a commonly used and well-tolerated anti-diabetic medication, has been recently investigated for its anti-neoplastic potential [21]. People with Type 2 Diabetes (T2D), a hypokinetic disease hallmarked by decreased insulin sensitivity and impaired glucose metabolism, are at a greater risk for developing cancer, but Metformin usage in patients with T2D is associated with a decreased risk of lung cancer [22]. In particular, NSCLC cancer patients with co-morbid T2D showed improved survival rates with prolonged Metformin usage [23].

Metformin is a widely used biguanide that controls hepatic gluconeogenesis through a variety of mechanisms [24, 25]. Metformin's canonical mechanism of action is inhibiting oxidative phosphorylation, driving an inhibition of hepatic gluconeogenesis and increasing β-

oxidation, particularly in skeletal muscle and liver tissue [24]. Specifically, Metformin is

transported into the mitochondria via an organic cation ion transporter (OCT 1), allowing

Metformin to enter the cytosol to then cross the outer and inner mitochondrial membrane [24].

Metformin accumulation in the mitochondria inhibits the Complex 1, a protein complex vital to

drive oxidative phosphorylation in the electron transport chain, resulting in a reduction in

NAD+/NADH oxidation and reduced ATP production [26, 27].   A decrease in ATP production

increases the ratio of adenosine monophosphate (AMP) to ATP or adenosine diphosphate (ADP)

to ATP, activating AMP activated protein kinase (AMPK). AMPK is an important cellular

energy sensor that promotes insulin sensitivity in peripheral tissues and reduced adipocyte

formation [24]. Increased insulin sensitivity promotes glucose uptake, reduces hepatic glucose

production, and leads to improved systemic glucose metabolism.

In skeletal muscle, Metformin delays satellite cell activation by preserving the satellite

cell pool in a lower metabolic state, sustaining quiescence [28]. Maintenance of the stem cell

population is crucial to preserve skeletal muscle mass, repair, and function [29]. Metformin also

increases peroxisome proliferator-activated receptor-coactivator-1α (PGC-1α) protein

expression, a transcriptional co-activator that is involved in mitochondrial biogenesis, glucose

metabolism, and muscle fiber type [30]. PGC-1α increases the expression of genes involved in

energy metabolism, which is thought to protect skeletal muscle from atrophy [31]. Specifically,

PGC-1α suppresses Forkhead Box O3 (FoxO3), a transcription factor that induces the expression

of ubiquitin-ligases involved in atrophy [31].

Metformin elicits anti-tumorigenic effects in many cancers, including prostate, colon,
breast, skin, and obesity-activated thyroid cancer [32-36]. In cancers, Metformin induces
alterations in cellular proliferation, apoptosis, cell cycle progression, and inflammatory responses
through signaling pathways such including AMPK, mechanistic target of rapamycin (mTOR), mitogen activated protein kinase (MAPK), and the nuclear factor kappa-light-chain-enhancer of activated B cells (NFkB) and signal transducer and activator of transcription 3 (STAT3) pathway [37-40]. The efficacy of Metformin treatment on cancer cells appears largely dependent upon the expression level of organic cation transporters (OCTs), which transports Metformin across cellular membranes [41]. Tissues lacking this gene or possessing

Figure 1.1.1. Metformin induced AMPK-dependent and AMPK-independent mechanisms of action in cancer [1].

mutated OCT genes will likely not respond to Metformin treatment as readily, leading to variable
effectiveness [42]. Because Metformin's canonical mechanism of action is through inhibition of
the electron transport chain, a large portion of cancer studies demonstrate Metformin's anti-
cancer action via AMPK- dependent mechanisms. Impaired mitochondrial function increases
AMP binding to AMPK and AMPK activation through phosphorylation at Threonine 172 by
liver kinase B 1 (LKB1) [43]. LKB-1-activation of AMPK phosphorylates and activates Tumor
sclerosis complex 1 and 2 (TSC 1/2) and negatively regulates mTOR activity, reducing cell

growth and proliferation [44]. Activated AMPK also induces cell cycle arrest through activation of protein 53 (p53), leading to upregulation of pro-apoptotic genes [45, 46]. In prostate cancer cells, Metformin increases the expression of Regulated in development and DNA damage responses (REDD1), promoting mTOR inhibition and cell cycle arrest [47]. In breast cancer cells, AMPK has also been shown to activate forkhead transcription factors (FOXO), a protein family which can act a tumor suppressor through promotion of cell cycle arrest, DNA damage repair, and apoptosis [36].

Although Metformin elicits a significant anti-neoplastic effect via AMPK activity, Metformin also combats tumorigenesis independently of AMPK [1]. Metformin curtails insulin and insulin like growth factor (IGF-1) in pancreatic cancer cells, leading to phosphatidylinositol-3,4,5-triphosphate (PIP3) recruitment and subsequent activation of Protein Kinase B/AKT [48]. AKT phosphorylates TSC1/2, rendering TSC1/2 inactive and hindering mTOR activity [49]. The AMPK-independent action of Metformin on NSCLC progression remains largely uncharacterized, which may be due to Metformin's primary role as an AMPK activator. Metformin stimulates a pro-apoptotic effect on lung cancer cells through apoptotic cytotoxicity and proteosomal degradation, evidenced by decreased expression surviving which is an inhibitor of apoptosis proteins (IAPs) [50]. IAPs tightly control cell proliferation and cell death and many cancers show increased expression of IAPs [50]. Metformin downregulates the survivin levels by inhibiting protein kinase A (PKA) and releases the brake holding off cell-death, promoting NSCLC degradation [50]. Metformin also induces apoptosis though activation of caspase-3 and Poly (ADP-ribose) polymerase (PARP) cleavage, both of which are hallmarks of cell-death [50].

Tumor-bearing mice can develop imbalances in the myogenic regulatory program, demonstrated by reduced protein synthesis and increased protein degradation through the

ubiquitin-proteasome system, a chief protein catabolism pathway [51]. Specifically in a Lewis

lung carcinoma mouse model, fundamental genes involved in the phosphatidylinositol 3-kinase

(PI3K)-protein kinase B (Akt) pathway were attenuated [52]. The PI3K/AKT pathway, which is

often constitutively active in tumor cells, plays an important role in cellular proliferation, growth,

metabolism, and protein synthesis [53]. Reduced expression of regulatory genes in the

PI3K/AKT pathway could lead to mitochondrial dysfunction and skeletal muscle wasting [52].

Importantly, Metformin treatment in tumor bearing rats decreases skeletal muscle wasting and

improves protein metabolism, attenuating cancer-induced cachexia [54].

Due to the projected burden of lung cancer diagnoses over the next decade, understanding

mechanisms by which Metformin influences NSCLC progression may lead to potential

therapeutic options for enriched targeted therapy. While Metformin demonstrates antineoplastic

effects via cell cycle arrest, the mechanism underlying this pharmaceutical's action on NSCLC

tumor development largely remains unclear. Limited published literature has fully elucidated the

oncogenic programming alternations Metformin elicits on NSCLC cell proliferation and survival

and how skeletal muscle health may be supported throughout this disease progression. The

results of this project will provide novel insight into NSCLC oncogenic programming alterations

that may be induced through Metformin treatment. Importantly, assessing how Metformin may

support skeletal muscle health throughout lung cancer progression could contribute clinical

meaningful improvements for cancer patients.

1.2 Innovation

This proposal is novel because it will add to the literature by characterizing Metformin's

mechanistic effect on NSCLC tumorigenesis *in vitro* and *in vivo*. Full characterization of

oncogenic programming alterations, including the apoptotic factors influencing Metformin's

anti-tumorigenic effect on NSCLC remains unclear. Weekly monitoring of tumor growth in all animals via the In Vivo Imaging System (IVIS) allows for a comprehensive analysis of tumor growth and Metformin's effect on tumor proliferation. This approach allows all mice to be followed throughout the entire study rather than sacrificing animals at distinct time points. Furthermore, the orthotopic injection of NSCLC into an immunocompetent mouse allows a more comprehensive understanding of how the entire biological system responds to NSCLC tumor progression. Importantly, this will allow investigation into the effect of NSCLC progression on skeletal muscle health, independent of inducing cachexia.

1.3 Specific Aims

The objective of this proposal is to determine whether Metformin reduces lung cancer tumor burden while maintaining skeletal muscle health. Lung cancer patients routinely undergo surgical procedures, chemotherapy, and/or radiation. These therapies can drive ongoing systemic issues, greatly hindering patient welfare and recovery timelines [7]. For example, chemotherapy and radiation induce deleterious systemic side-effects, particularly within skeletal muscle. Chemotherapy and radiation patients suffer from muscle wasting characterized by increased protein degradation and reduced protein synthesis. The mechanisms are believed to include the destruction of skeletal muscle satellite cells, which leads to reduced potential for muscle repair and the maintenance of structure and function. Consequently, patients experience a decrease in quality of life, even in remission [9]. Therefore, the development of therapeutic interventions that preserve the integrity of skeletal muscle health are paramount to optimal treatment.

We hypothesize Metformin will reduce tumor burden and preserve skeletal muscle health in mice with NSCLC. Metformin, a commonly used and well-tolerated anti-diabetic medication,

has been more recently investigated for its anti-neoplastic potential [21]. Intriguingly, Type 2 Diabetic (T2D) patients treated with Metformin have a decreased risk of lung cancer [22] and NSCLC patients with co-morbid T2D have increased survival rates with prolonged Metformin usage [23]. Furthermore, Metformin increases the expression of peroxisome proliferator-activated receptor-coactivator-1α (PGC-1α), a transcriptional co-activator that protects skeletal muscle from atrophy [31]. Metformin also delays satellite cell activation by preserving the satellite cell pool in a lower metabolic state, sustaining quiescence [28]. Maintenance of the stem cell population is crucial to preserve skeletal muscle mass, repair, and function [29].

Our hypothesis will be tested through the following aims:

Specific Aim 1: Determine whether Metformin reduces NSCLC tumor burden. We will test this aim using live animal imaging of NSCLC tumor growth in mice treated with Metformin or vehicle. We hypothesize that mice treated with Metformin will have reduced tumor burden, maintain body mass, and have increased survival.

Specific Aim 2: Determine whether Metformin supports skeletal muscle health in mice with NSCLC. We will test this aim by examining changes in the expression of cellular and molecular regulators of skeletal muscle mass and metabolism. We hypothesize that Metformin treatment will increase PGC-1alpha expression and decrease STAT3 expression. We anticipate that Metformin treatment will improve metabolism though increased expression of regulatory genes in the PI3k/AKT pathway.

Specific Aim 3: Determine the mechanisms by which Metformin alters the oncogenic program of NSCLC. We will test this aim using an *in vitro* approach to quantify the effect of Metformin on NSCLC proliferation and the expression of oncogenic regulators. We hypothesize that Metformin will reduce NSCLC proliferation through decreased expression of mTOR and

increased expression of REDD1. We anticipate Metformin to induce apoptosis though increased expression of caspase 3, p53 and Ki-67.

1.4 Pilot Work

Lewis Lung Carcinoma (LL/2) cells, a NSCLC cell line that stably harbors luciferase reporter expression (Imanis Life Sciences), were utilized for these experiments. LL/2cells are a commonly used lung cancer model that share a genetic background with C57BL/6 mice, a well-defined immunocompetent mouse model for cancer [55, 56]. We performed a pilot study to validate the luciferase reporter expression *in vitro*. The luciferase reporter in our LL/2 cell line is detectable with the IVIS system following injection of D-luciferin (150ug/ml) *in vitro* and incubation at 37°C for a short period of time (Figure 1.4a). We also performed a pilot study to validate the luciferase reporter expression and maximize tumor visibility *in vivo*. Because published literature shows a wide range

Negative Control   **Positive Control**

Figure 1.4.1. Luciferase reporter expression in Lewis Lung Carcinoma Cells. Image confirming the luciferase reporter expression in Lewis Lung Carcinoma (LL/2) cells. following exposure to D-luciferin *in vitro*.

of orthotopic lung cancer concentrations, tumor cells were subcutaneously injected at final concentrations of 1,000, 10,000, and 100,000 cells into different mice [57-59]. Mice were given an injection of D-luciferin (150mg/kg) 15 minutes prior to imaging and images were captured at two time points prior within one hour of the D-luciferin injection.

We determined the optimal concentration of LL/2 cells *in vivo* to be 1,000 LL/2 cells (Figure 1.4.b). Although 1,000 LL/2 cells were not readily detectable through IVIS imaging, using a lower concentration of cells could

Figure 1.4.2. Images confirming the Lewis Lung Carcinoma (LL/2) luciferase reporter expression *in vivo*. From left to right, 1,000, 10,000, and 100,000 LL/2 cells subcutaneously injected into three C57BL/6 mice and visualized using D-luciferin.
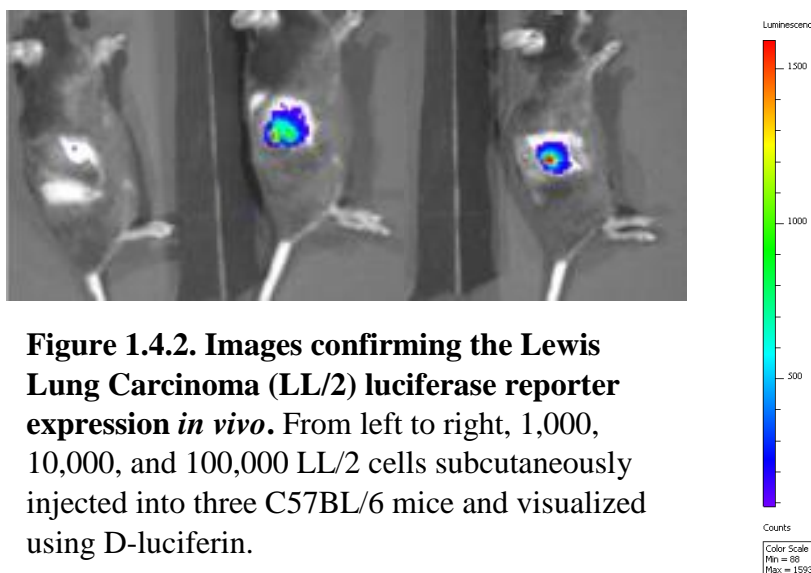
improve the longevity of the study by allowing tumor burden to progress at a slower pace and preventing a rapid overburden of the animal's system. Concentrations greater than 10,000 LL/2 cells caused aggressive tumor burden in mice initiating a rapid decline in survival. We assessed tumor growth in one male and one female C57BL/6 mouse using an orthotopic injection of 1,000 LL/2 cells over a period of 5 weeks and in combination with Metformin treatment (250 mg/kg) (Figure 1.4c).

Our preliminary work confirmed the detection of bioluminescent signal *in vivo*, demonstrated that LL/2 cells are compatible with an immunocompetent mouse model, and allowed us to establish an optimal concentration of LL/2 cells to orthotopically inject into C57BL/6 mice. Through the proposed work, we are aiming to

Figure 1.4.3. Images confirming the Lewis Lung Carcinoma (LL/2) luciferase reporter expression following 5 weeks of lung cancer and Metformin treatment. One male (left) and one female (middle) left lung (right) from C57BL/6 mice injected with LL/2 cells. LL/2 cells were visualized using D-luciferin.
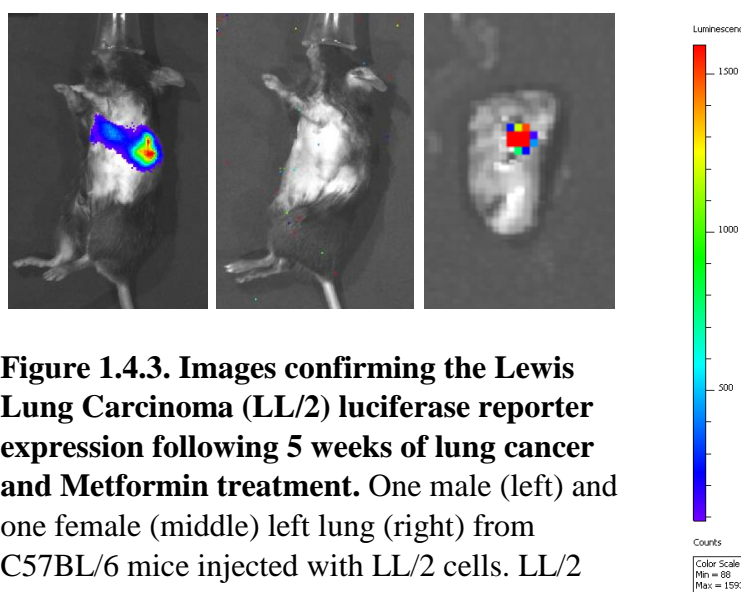
determine the efficacy of Metformin in the treatment of NSCLC. Understanding mechanisms by

which Metformin influences NSCLC progression could lead to potential therapeutic options for

enriched targeted therapy. Importantly, assessing how Metformin may support skeletal muscle

health throughout lung cancer progression could contribute clinical meaningful improvements

for cancer patients.

CHAPTER 2: EFFECTS OF METFORMIN TREATMENT ON LL/2 TUMOR BURDEN IN

C57BL/6 MICE

2.1 Introduction

Lung cancer is the second most common cancer and represents ~13% of all new cancer

cases in the United States (SEER, National Cancer Institute). Lung cancer contributed to

~145,000 fatalities in 2019 [60], with the yearly diagnoses expected to reach 225,000 in 2030,

just in the United States alone [3]. Cigarette smoke has been one of the largest contributors to

lung cancer diagnoses, but now it is established that a combination of lifestyle, genetic, and

environmental components contribute to an individual's risk and development of lung cancer [4].

Specifically, factors which can put individuals at a greater risk for lung cancer include cigarette

smoke, environmental pollutants, alcohol consumption, adverse dietary consideration, physical

inactivity, and hereditary markers [4].

Lung cancer patients have a 5-year relative survival rate of only 19% (16% for men and

22% for women) [2]. While the 5-year relative survival rate for these patients has slightly

increased over the last 37 years, the relative five-year survival rate remains close to 20% (SEER

National Cancer Institute), making it one of the lower survival rates among cancers. While

treatments continue to improve, the prevalence and severity of lung cancer necessitates more

refinement of treatment modalities.

Continuous advances are bringing new insight into oncology therapeutics [18] and in

particular, through drug repositioning [46]. This is attractive tactic since new drug

characterization and approval requires extensive monies, time, and investment [19].

Observational studies, pre-clinical trials, and clinical trials have provided insight into the efficacy

of drug repositioning both for cancer prevention and cancer therapy [20].

Metformin canonically facilitates improved insulin sensitivity and overall glucose uptake for Type 2 Diabetic (T2D) patients, but recent studies show the potential of repositioning Metformin due to its anti-cancer properties [32, 33, 36, 61, 62]. Importantly, literature suggests that Metformin decreases lung cancer risk for T2D patients and increases survival for lung cancer patients with co-morbid T2D [22, 63-65]. Metformin elicits anti-tumorigenic effects in many cancers, including prostate, colon, skin, and obesity-activated thyroid cancer [32-35]. In cancers, many signaling pathways including AMPK, mTOR, MAPK, and insulin-like growth factors contribute to the anti-tumorigenic effects of Metformin [37]. In particular, Metformin activates AMPK inhibiting cell mitosis and proliferation, particularly via protein p53 activation [46]. While Metformin demonstrates antineoplastic effects via cell cycle arrest, the efficacy of Metformin and the mechanism underlying this pharmaceutical's action on NSCLC tumor development remains unclear. Understanding this gap in the literature is crucial to the careful repositioning of Metformin as an anti-cancer therapeutic. Utilizing Metformin independently or in conjugation with other treatment modalities could mitigate side effects many cancer patients experience while receiving more potent oncology therapeutics.

Although Metformin has been used as an anti-cancer therapy in clinical trials, Metformin's efficacy on NSCLC remains understudied, requiring further investigation into the potential effectiveness of this therapeutic. The purpose of this study was to determine whether Metformin treatment suppresses tumor growth in C57BL/6 mice with NSCLC. Determining the efficacy of Metformin therapy for NSCLC could augment therapeutic options for cancer patients and provide valuable insight into physiological disparities underlying NSCLC progression.

2.2 Experimental Design and Methods

2.2.1 Experimental Animals

Six week-old male (n=12) and female (n=12) C57BL/6j mice (Jackson Laboratory, Bar Harbor, ME) were randomly assigned into a control group (lung cancer without Metformin treatment) (n=12; 6 males, 6 females) and a Metformin treatment group (lung cancer with Metformin treatment) (n=12; 6 males, 6 females). Control (n=7) and Metformin (n=9) animals completed the study and were used in statistical calculations. Some control mice (n=5) and Metformin mice (n=3) mice presented extreme tumor burden and did not survive for the full length of study and were excluded from statistical calculations (Table 2.6.1). Figure 2.5.1 outlines the study progression.

All mice were provided with *ad libitum* access to water and standard rodent chow (Teklad Diets 2919, Envigo). Food mass was measured weekly and the total amount of food consumed over the study was used to determine total caloric intake. The energy density of the standard rodent chow was 3.3 kcal/g. Male and female C57BL/6 mice were used to address Metformin's efficacy on reducing lung tumor burden in immunocompetent mice. We used the Lewis Lung Carcinoma immunocompetent mouse model to mimic lung tumor development including the immune system modulations. The non-small cell lung carcinoma (NSCLC) Lewis Lung Carcinoma (LL/2) cells is syngeneic with C57BL/6 mice and stably and constitutively expresses a luciferase reporter (Imanis Life Sciences). All aspects of this study were approved by the Institutional Animal Care and Use Committee at the University of North Carolina at Charlotte.

2.2.2 Culturing Non-Small Cell Lung Cancer Cells

NSCLC cells (Imanis Life Sciences) were grown in standard growth media (Dulbecco's Modified Eagle Medium) with 10% fetal bovine serum and 1% penicillin-streptomycin. Cells

were passaged with 2µg/ml puromycin to maintain high luciferase fluorescence expression. Cells were maintained at 37°C for 48 hours or until predetermined time points.

2.2.3 Orthotopic Injection

Animal hairs were removed and the ventral and left thoracic regions were aseptically prepared. Prior to receiving an LL/2 cancer injection, all animals were imaged and baseline images acquired using the In Vivo Imaging System (IVIS). Under anesthesia (1-3% isoflurane), mice received one orthotopic lung injection of LL/2 cells into the left lung. LL/2 cells (1.0×10^3) were administered in PBS and Matrigel® (10µg; Dulbecco's Modified Eagle's Medium with 50ug/mL gentamycin Phenol Red Free, Corning). Matrigel® facilitated both tumor cell growth and homing within the lung tissue [66]. A small incision (3-5mm) was made to expose the area surrounding the seventh and eighth ribs. Cells were injected orthotopically into the lung using a sterile 29-gauge syringe and the incision was closed with a wound clip. Following surgery, all mice were individually housed and allowed to recover for one week. Animal weights were recorded weekly throughout the study. Any mice showing signs of distress or exceeding 20% body mass loss, in accordance with approved IACUC guidelines, were euthanized to maintain humane endpoints for all animals.

2.2.4 *In Vivo* Imaging

Tumor growth in all animals was initially monitored weekly using bioluminescent imaging via the In Vitro Imaging System (IVIS). Cell visualization *in vivo* occurred by giving all animals D-luciferin (150mg/kg) 15 minutes prior to imaging. The area to be imaged was shaved and cleaned to remove any hair that could interfere with the bioluminescent signal detected. All images were captured within a 30 minute window following D-luciferin injection.

All mice were imaged weekly until a bioluminescent signal was detected. Follow detection, each mouse continued bi-weekly imaging and began treatment.

2.2.5 Metformin Treatment

Control and Metformin-treated mice were injected intraperitoneally (i.p.) with saline and Metformin (250mg/kg, twice weekly). Metformin Hydrochloride (1084; Sigma Aldrich) was dissolved in 1x phosphate buffered saline (PBS) and sterile filtered (0.2µm) for a final dose of 250mg/kg. Metformin was cultured on nutrient agar plates to ensure no visible contaminants were present. Metformin mice received 250mg/kg Metformin via intraperitoneal (i.p.) injection twice a week [39, 67]. Control mice received a placebo of 1x phosphate buffered saline (PBS) solution via an i.p. injection twice a week. 5-week post-tumor implantation, mice were euthanized (>4% isoflurane), and tissues collected, snap frozen on liquid nitrogen, and stored at -80°C.

2.2.6 Tumor Burden

Tumor burden was assessed with the Living Image analysis. The region of interest (ROI) was determined by outlining the tumor bioluminescent signal with minimum detection parameters set to 5%. Brightness, contrast, and opacity were maintained between all images regardless of time point. A separate ROI was drawn on each mouse to determine background signal. Mice with metastases were identified by more than ROI at a single time point. Each bioluminescent signal was first normalized to the background signal for the same image. All animals were normalized to the baseline image of the same mouse. Total counts for animals with multiple detectable bioluminescent signals were added together to determine total tumor burden for a single mouse at a single timepoint. Mice with a saturated signal were excluded from analyses.

2.2.7 Tumor Tissue Homogenization and mRNA extraction

Tumor tissue (≤30mg) was placed into a microcentrifuge tube with beads in ~300 ul (or sufficient volume not exceeding 10% of tissue mass) QIAzol lysis reagent (79306; Qiagen). Tissue was disrupted with a bead blaster homogenizer (BeadBlasterTM 24 Microtube, Sigma) with 2 separate rounds of 2-30 second intervals at 619 meters/second followed by 1 minute of rest. Following lysis, mRNA was extracted utilizing a RNeasy Lipid Tissue Mini Kit (74804; Qiagen). Following the addition of chloroform, the upper aqueous phase was removed and placed into a clean tube and washed multiple times. mRNA from homogenized tissue was eluted using RNAse-free water though a RNeasy column. The quality and quantity of mRNA was assessed using NanoDrop 1000. Briefly, 2uL of RNAse-free water was used to blank the NanoDrop. 2uL of sample was loaded onto the pedestal and quantified. Quality of mRNA was determined using the 260/280 and 260/230 ratios.

2.2.8 cDNA and Real-time PCR

Real-time polymerase chain reaction (PCR) (qPRC) was used to evaluate gene expression targets involved in cell cycle regulation and tumor suppression. Regulators of the cell cycle included cyclin D kinase 4 (CDK4) and protein 27 (p27). Tumor suppression targets included protein 21 (p21). F4/80, a macrophage marker, and hairy and enhancer of Split-1 (HES1), a downstream target gene involved in cellular determination and fate, were also included in analyses. Briefly, Radiant Green HI-ROX SYBR Green was utilized for all real-time qPCR. Glyceraldehyde 3-phosphate (GAPDH) was the housekeeping gene for all qPCR experiments. SYBR green ROX cycling occurred under the following conditions: cDNA was activated at 95°C for 2 minutes followed by 20 cycles of 95°C for 5 seconds (denaturation) and 60°C for 20 seconds (annealing/extension).

2.2.9 Statistical Analyses

An unpaired t-test was used to assess baseline body mass between all control and Metformin mice. A mixed-effects model (time x treatment) was use to assess normalized body mass between treatment groups and food consumption for the duration of the study. An unpaired t-test was used to identify any differences in time to caloric intake, signal detection, and length of treatment. Overall survival was determined by a Logrank test. An unpaired t-test was used to identify gene expression differences between control and treatment animals. Outliers were identified using a Grubb's test. Significance will be established with an *a priori* alpha value of 0.05. All statistics will be completed in GraphPad Prism (Version 9.1).

2.3 Results

2.3.1 Body Mass in C57BL/6 Mice with NSCLC

The unpaired t-test revealed no differences in baseline body mass between control and Metformin mice (p = 0.734). As expected, control and Metformin animals increased in body mass through the duration of the study (Figure 2.5.2). Mixed modeling (time x treatment) from all mice with a detectable bioluminescent signal indicated significant increases in body mass with time [$F(2.320, 27.85) = 8.788, p < 0.001$] but not treatment [$F(1, 14) = 4.510, p = 0.0520$] or an interaction (time x treatment) effect [$F(5, 60) = 1.943, p = 0.1005$]. There were no differences detected between male and female cohorts, justifying the comparison of treatment cohorts including both sexes rather than separating into smaller samples sizes based off gender. Since body mass was not significantly different at baseline body mass was represented as a fold change from baseline.

2.3.2 Food Consumption in C57BL/6 Mice with NSCLC

Control and Metformin animals continued consuming food for the duration of the study (Figure 2.5.3). Mixed modeling (time x treatment) indicated significant increases in food consumption with time [F (2.472, 40.38) = 11.32, $p < 0.0001$], independent of treatment. Control mice had significantly lower (p=0.018) total caloric consumption compared to Metformin animals (Figure 2.5.3).

2.3.3 Time to Tumor Detection and Length of Treatment

An unpaired t-test revealed differences over overall time to a detectable bioluminescent signal between control and Metformin animals (p=0.790) (Figure 2.5.4). The length of treatment between cohorts remained similar, irrespective of treatment (p=0.753) (Figure 2.5.5).

2.3.4. NSCLC Tumor Burden and Animal Survival

The mean survival for control (37±5.6 days) and Metformin (40±1.4 days) groups were not statistically significant (Figure 2.5.5). The Welch's t-test revealed no significant differences in mean survival time between groups (p=0.412). The log rank test revealed no differences in overall survival between control or Metformin treated mice with a detectable bioluminescent signal (p=0.827) (Figure 2.5.6). No statistically significant trends were identified between cohorts (p = 0.0515). The unpaired t-test revealed a similar tumor burden signal in each group, irrespective of treatment (p=) (Figure 2.5.7). Representative images of LL/2 tumor signal in a female control and male Metformin mouse can be seen in Figure 2.5.8.

2.3.5 NSCLC Tumor Gene Expression

Unpaired t-tests revealed no significant differences in gene expression in NSCLC tumors from C57BL/6 mice. Within tumors, p27, CDK4, F480, IL-6 or Hes1 gene expression were similar between control and Metformin treated mice (p27, p 0.639; CDK4, p=0.973; F480,

p=0.488; IL-6, p=0.203; Hes1, p=0.118) (Figure 2.5.9). However, Hes1 expression shows a modest significant effect for sex when males and females are separated within each treatment group [$F(1, 8) = 6.828$; p=0.031].

2.4 Discussion and Conclusion

The present study aimed to assess the effects of Metformin as stand-alone treatment in altering LL/2 tumor progression in C57BL/6 mice. The data obtained highlight that the regimen used (250 mg/kg, twice weekly, IP) in an immunocompetent model of NSCLC was not associated with significant improvement in tumor burden, or marked change in key tumor cell division and inflammation markers: namely, cell cycle regulatory (p27, CDK4 and Hes1) and inflammation (F4/80 and IL-6) gene expression within the tumor were not significantly altered by Metformin treatment.

The LL/2 orthotopic model effectively mimics lung cancer growth and tumor burden in accordance with other murine Lewis lung cancer models [55, 66, 68]. The LL/2 cells with a bioluminescent marker allowed tracking tumor growth (IVIS imaging) limiting the number of animals used and the monitoring of tumor growth over time.

All gene expression analyses were grouped based off treatment rather than separating via sex to ensure adequate sample sizes for the scope of this project. If animals are separated by sex within each group, Hes1 gene expression shows a small significant effect for sex (p=0.031). In the present study, male mice showed reduced Hes1 expression when compared to female mice; however, the sample size for tumor tissue from cancer-bearing mice remains very small (males, n=2; females, n=4 per treatment group). In light of this limited scope, this potential significance suggesting that Hes1 regulation may be variable between male and female mice and could influence potential sex-related differences in downstream cellular fate is trivial at best. While no

significant differences in tumor fold change or cell cycle regulatory genes (p27 and CDK4) were identified between the control and Metformin treated mice, this could be a result of an insufficient frequency of Metformin administration throughout the study. Metformin has a relatively short half-life, a high rate of absorption in the small intestine, and a nearly complete clearance via the kidneys, indicating that bioavailability of Metformin is limited and drug delivery to the tumor site is inadequate [69, 70]. Appropriate delivery of the anti-cancer therapeutic is of utmost importance. A better route of administration could be through oral administration via drinking water. Delivering medicines through drinking water results in more consistent drug levels in the plasma when compared to drug delivery via IP injections [71, 72] Mice treated with Metformin through drinking water, rather than IP injections, lead to an average of 32µM (range of 9.1-55.7µM) in blood plasma levels, allowing more consistent drug delivery to the tumor site [71].

Notably, the application of nanoparticle technology has provided an advantageous approach to more innovative cancer treatments. The modernization of nanoparticle gene therapy technology allows encapsulation, complexation, or surface loading of DNA and RNA sequences by artificial polymers, proteins, lipids or polysaccharides [73]. Nanocarriers possess many unique characteristics, making them excellent vehicles for drug delivery with the potential to better regulate pharmacokinetic effects [74]. This leads to improved uptake of a nanoparticle into a target cell, resulting in increased bioavailability of the drug, more controlled release of a therapeutic, increased stability of the drug, and reduced side-effects from more conventional cancer treatments [75]. For many years, nanoparticle gene therapy *in vitro* and *in vivo* proves to be an effective route for both cellular transfection and targeting lung cancer tumors, systemically and locally [73]. Specifically in NSCLC lines, nanoparticle carriers encapsulated biomolecules

and successfully reached target tissues, resulting in either silencing or knockdown of genes to attenuate tumor cell growth [76, 77]. However, nanoparticle delivery does provide some challenges as these platforms are implemented into the clinical population. In particular, the stability of the nanoparticle upon delivery, penetrability of larger biological membranes, the potential cytotoxicity from the nanoparticles, and the heterogeneity of nanoparticles required for specific drug delivery.

Although there was not a significant reduction in F4/80 or IL-6 gene expression, animals receiving Metformin treatment trended toward a lower IL-6 gene expression. IL-6 is a multifaceted cytokine that acts as a key mediator of inflammation. High serum concentrations of IL-6 are associated with tumor progression, metastases, and poor clinical outcomes, especially for colorectal cancer patients [78]. In lung cancer patients, Metformin has also been shown to reduce IL-6 driven epithelial-mesenchymal transitions, which plays an important role in tumorigenesis [79]. Together these findings suggest that Metformin may play a role in mitigating tumor migration through IL-6.

Metformin has been shown to reduce infiltration of tumor-associated inflammatory macrophages [80]. A previous study indicated that Metformin (0.5-2.0 mM *in vitro*; 100mg/kg/daily *in vivo*) blocked alternatively activated (M2) macrophage polarization, which is often associated with tumor-driven angiogenesis, tumor migration and invasion, and suppression of anti-tumor immune responses [80]. Interestingly, Metformin also reduced Lewis lung cancer metastases without affecting tumor growth *in vivo* [80]. This suggests that while Metformin may not be directly targeting the tumor growth, Metformin is affecting the tumor microenvironment, possibly mitigating metastases. Low-dose metformin (50mg/kg/day) administration in esophageal squamous cell carcinoma did not affect proliferation or apoptosis of cancer cells, but

Metformin treatment increased tumor-suppressing macrophages *in vitro* [81]. Similarly, low-dose Metformin (250mg/day) leads to reprogramming the tumor immune microenvironment in humans with esophageal cancer [81]. It appears that Metformin may play a more significant role in modulation of the tumor microenvironment rather than have a direct anti-tumorigenic impact on the tumor cells, particularly for prostate cancer cells [82].

Metformin administration to cancer cells *in vitro* has shown hopeful anti-neoplastic potential, but the effect appears inconsistent with some *in vivo* findings. However, Metformin maybe be supportive in adjuvant therapies or in combination with more potent cancer drugs. Future studies should include a more frequent dosing of Metformin, alternate routes of drug administration, and potential combination therapies to enhance Metformin's potential as a tumor suppressor.

2.5 Figures
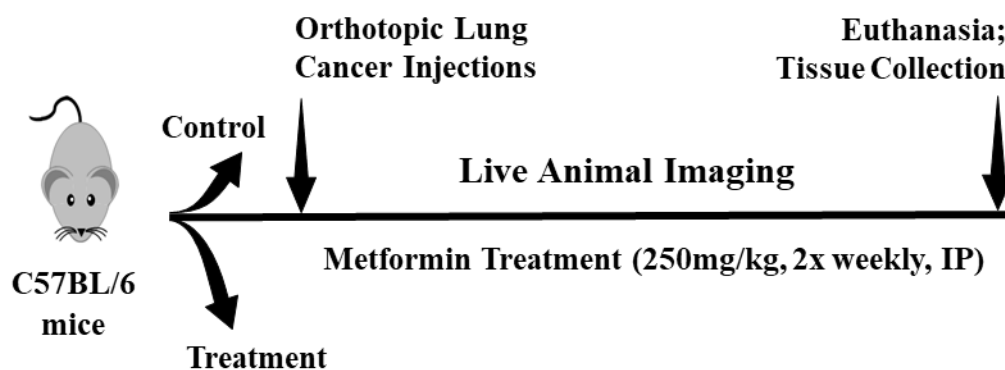
Figure 2.5.1. Experimental timeline for Lewis Lung Carcinoma Development in an Immunocompetent Mouse Model. Male (n=12) and female (n=12) C57BL/6 mice received 1,000 Lewis Lung Carcinoma cells harboring luciferase reporter expression. Live animal imaging continue for the duration of the study. Once a bioluminescent signal was detected, vehicle or Metformin treatment (250mg/kg, 2x weekly, Intraperitoneal injection) began.

A)

B)
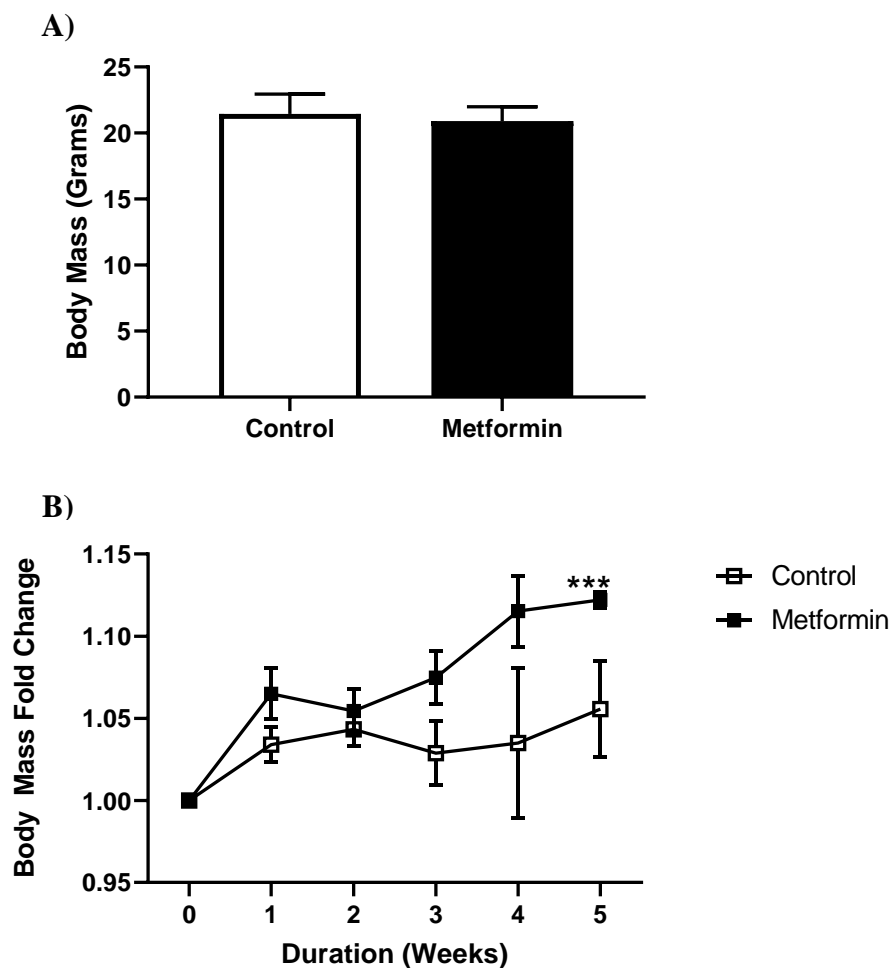
Figure 2.5.2. Body Weight in C57BL/6 Male and Female Mice. A) Body mass (grams) between control and treatment mice. B) Body mass fold change between control and Metformin (250mg/kg) treated mice following orthotopic LL/2 injection. Data were analyzed using mixed modeling (time x treatment). ***$p<0.001$, main effect for time. Control, n=7; Metformin, n=7. Data are mean ± SEM.

A)

B)
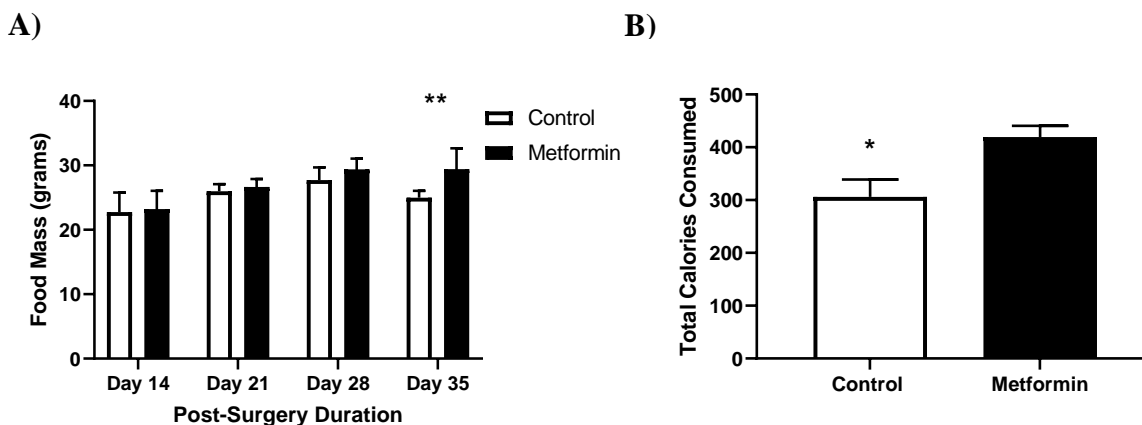
Figure 2.5.3. Total Food Mass and Caloric Consumption in C57BL/6 Male and Female Mice following Lung Cancer Injection. A) Food consumption (grams) between control and treatment mice following tumor injection. Data were analyzed using mixed modeling (time x treatment). ** $p<0.0001$, main effect for time compared to Day 14. Control, n=7; Metformin, n=8. Data are mean ± SEM. B) Caloric Consumption between control and Metformin (250mg/kg) treated mice following orthotopic LL/2 injection. Data were analyzed using an unpaired t-test. *$p=0.018$ compared to Metformin animals. Control, n=7; Metformin, n=6. Data are mean ± SEM.
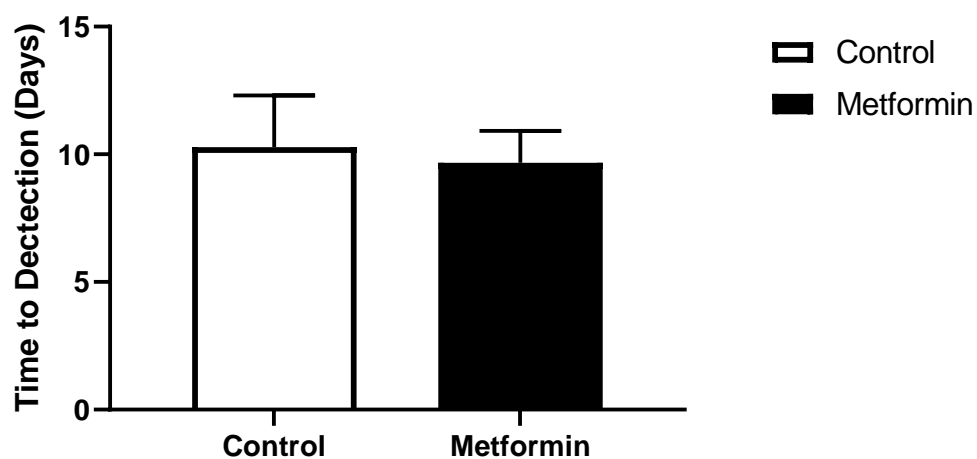
Figure 2.5.4. Time to Tumor Detection in C57BL/6 Male and Female Mice following Lung Cancer Injection. The number of days to discern an bioluminescent signal following orthotopic injection of LL/2 cells into C57BL/6 mice. Data were analyzed using an unpaired t-test. Control, n=7; Metformin, n=9. Data are mean ± SEM.
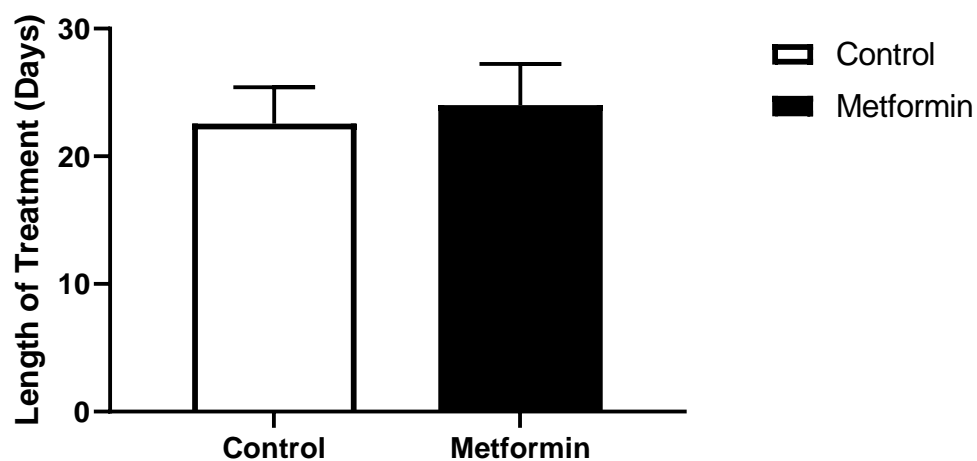
Figure 2.5.5. Length of Treatment in C57BL/6 Male and Female Mice following Lung Cancer Injection. The number of days C57BL/6 mice with NSCLC underwent treatment with control or Metformin (250mg/kg). Data were analyzed using an unpaired t-test. Control, n=7; Metformin, n=6. Data are mean ± SEM.
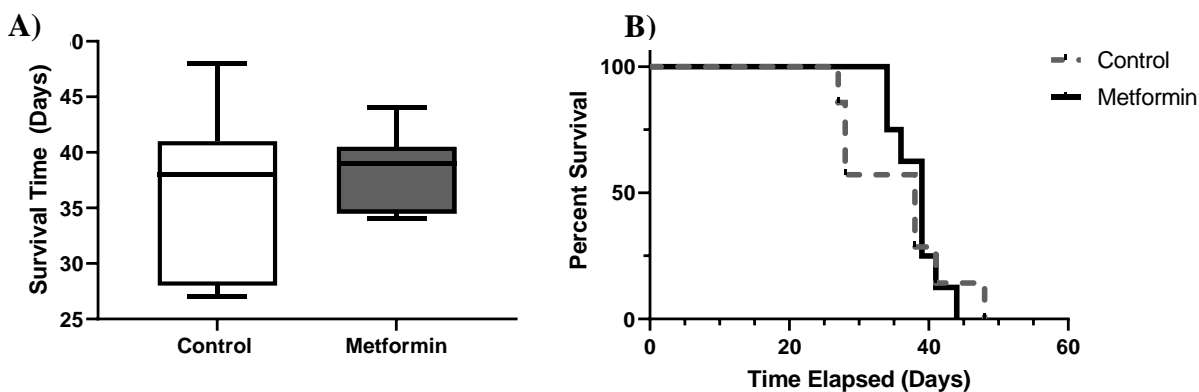
Figure 2.5.6. Survival Time in C57BL/6 Male and Female Mice following Lung Cancer Injection. A) Survival duration (days) between control and Metformin (250mg/kg) treated mice with a detectable bioluminescent signal. Data were analyzed with a Welch's t-test. B) Percent survival of both control and Metformin (250mg/kg) treated mice following detection of a bioluminescent signal. Data were analyzed with a Log-rank test. Control, n=7; Metformin, n=8. Data are mean ± SEM.
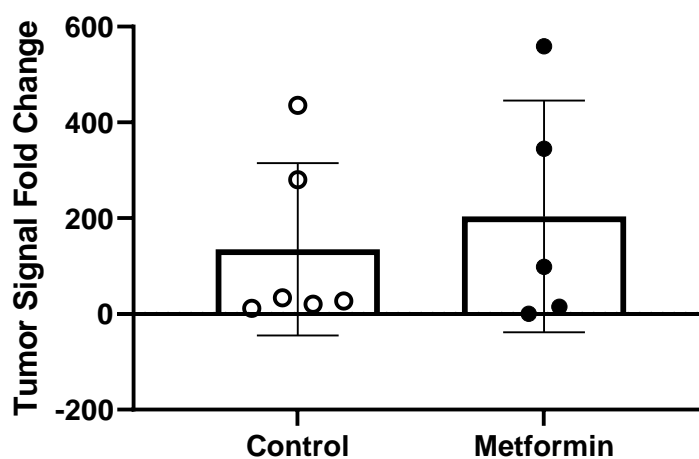
Figure 2.5.7. Tumor Burden in C57BL/6 Male and Female Mice following Lung Cancer Injection. NSCLC tumor burden fold change between control and Metformin (250mg/kg) treated mice with a detectable bioluminescent signal. Mice with a saturated signal were removed from analyses. Data were analyzed with a Welch's t-test. Control, n=6; Metformin, n=5. Data are mean ± SEM.
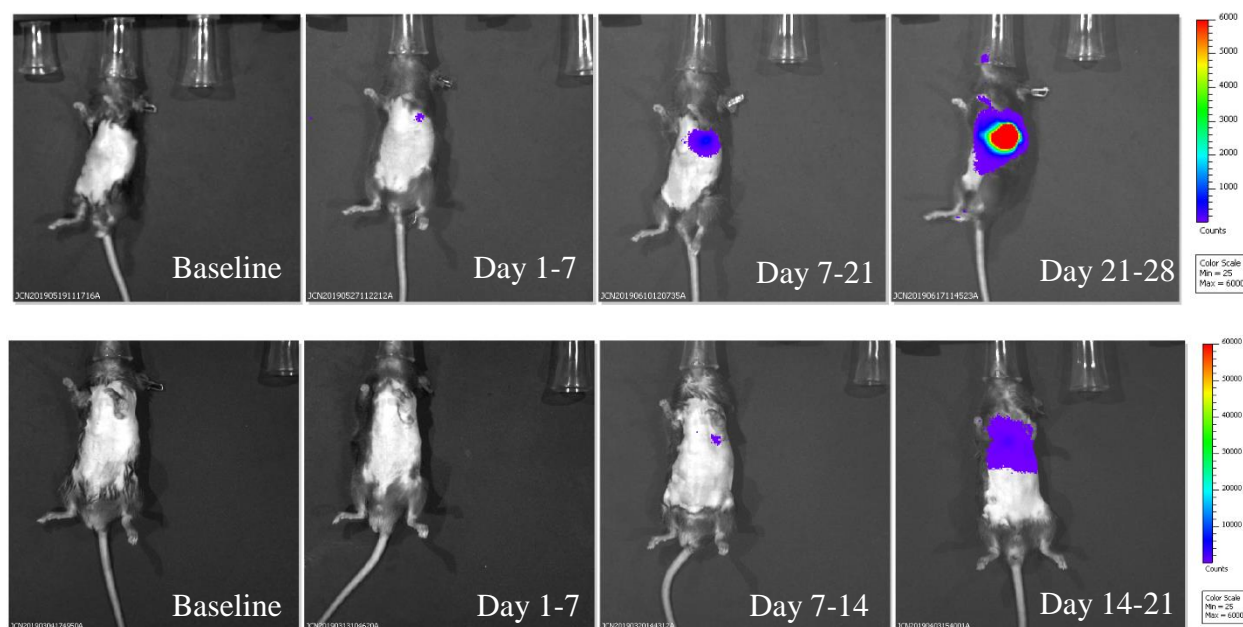
Figure 2.5.8. Non-Small Cell Lung Tumor Growth in C57BL/6 Male and Female Mice following Lung Cancer Injection. Male (n=12) and female (n=12) C57BL/6 mice received 1,000 Lewis Lung Carcinoma cells harboring luciferase reporter expression. Bioluminescent signals were tracked throughout the duration of the study via the In Vivo Imaging System. Once a bioluminescent signal was detected, vehicle or Metformin treatment (250mg/kg, 2x weekly, Intraperitoneal injection) began. Top row: Control C57BL/6 female mouse; Bottom row: Metformin C57BL/6 male mouse.

A)

B)

C)

D)

E)
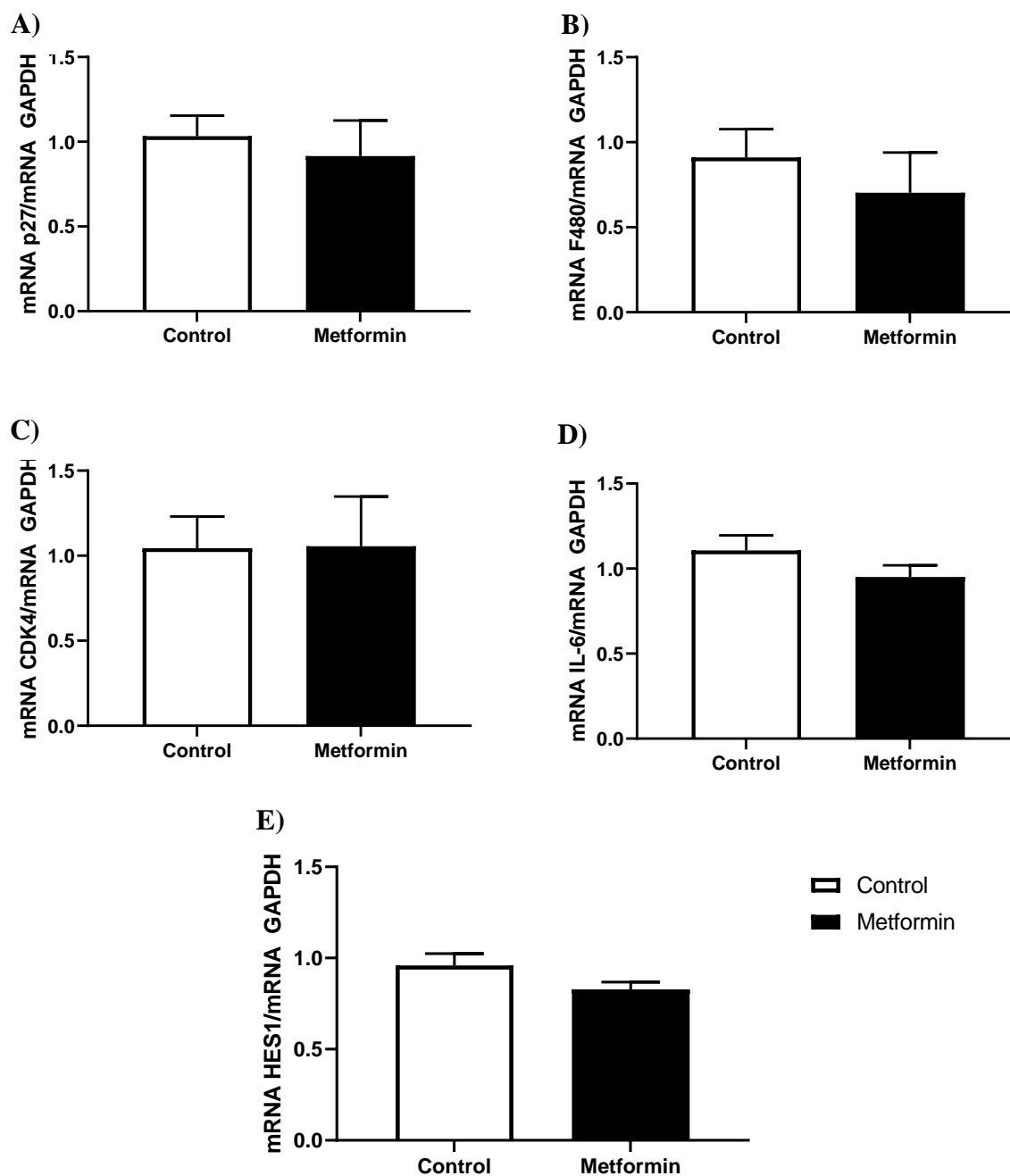
Figure 2.5.9. Tumor Gene Expression in C57BL/6 Male and Female Mice following Lung Cancer Injection. A) mRNA cyclin dependent kinase inhibitor (p27)/GAPDH; B) mRNA F480/GAPDH; C) mRNA cyclin dependent kinase (CDK4)/GAPDH; D) mRNA hairy and enhancer of split 1 (Hes1)/GAPDH. Tumor mRNA expression from C57BL/6 mice with NSCLC concomitant with or without Metformin (250mg/kg) treatment. Data were analyzed using an unpaired t-test. Sample size: Control, n=6; Metformin, n=6. Data are mean ± SEM.

Table 2.6.1. C57Bl/6j Mice Survival and Metastases following Injection with LL/2 cells.

Group	Mice began study, n	Mice survived, n	Mice with signal, n	Mice with metastases, n
Males	6	3	3	2
Females	6	4	4	1
Total Control	**12**	**7**	**7**	**3**
Males	6	3	3	0
Females	6	6	6	3
Total Metformin	**12**	**9**	**9**	**3**

Table 2.6.2 Primers used for Gene Expression Analyses.

Primer		Sequence
p27	Forward	TCTCTTCGGCCCGGTCAAT
	Reverse	AAATTCCACTTGCGCTGACTC
F4/80	Forward	CTTTGGCTATGGGCTTCCAGTC
	Reverse	GCAAGGAGGACAGAGTTTATCGTG
CDK4	Forward	ATGGCTGCCACTCGATATGAA
	Reverse	TCCTCCATTAGGAACTCTCACAC
IL-6	Forward	CTGCAAGAGCTTCCATCCAGTT
	Reverse	GAAGTAGGGAAGGCCGTGG
Hes1	Forward	GGTCCTGGAATAGTGCTACCG
	Reverse	CACCGGGGAGGAGGAATTTTT
GAPDH	Forward	ATGTTTGTGATGGGTGTGAA
	Reverse	ATGCCAAAGTTGTCATGGAT

p27: cyclin dependent kinase inhibitor protein 27; CDK4: Cyclin dependent kinase 4; IL-6: Interleukin 6; Hes1: Hairy and enhancer split protein; GAPDH: Glyceraldehyde 3-Phosphate Dehydrogenase

CHAPTER 3: EFFECTS OF METFORMIN TREATMENT ON SKELETAL MUSCLE

HEALTH FOLLOWING LL/2 TUMOR GROWTH IN C57BL/6 MICE

3.1 Introduction

Non-small cell lung cancer (NSCLC) makes up 80-85% of all new cancer diagnoses [4].

Following diagnoses, lung cancer patients often undergo surgical procedures, chemotherapy, or

radiation to combat cancer progression, but these therapies can drive ongoing systemic problems,

greatly hindering patient welfare and recovery timelines. One of the largest systemic effects of

cancer treatment with these conventional methods is cachexia, the rapid loss of skeletal muscle

and adipose tissue [10, 11].

Cachexia, which is characterized by systemic inflammation, involuntary loss of lean

muscle, insulin resistance, and a staunch negative energy and protein balance, [83, 84] occurs in

more than 50% of lung cancer patients undergoing chemotherapy or radiotherapy or a

combination of both [12, 13]. More than 60% of patients with advanced NSCLC can present

respiratory complications and increased rates of cachexia [85]. Patients with cancer-induced

cachexia often present a lower tolerance and responsiveness to chemotherapy, shortened survival

time, and a far greater symptom burden [86]. A higher morbidity and mortality rate is also

correlated with a more prominent weight loss and rapid decrease in BMI, both of which are

independent prognostic factors for cancer patients, with or without cachexia [85, 87]. Few

treatment options are available for cachexia and these induced effects are irreversible even

during remission, making the repercussions even more debilitating [9, 15].

Skeletal muscle, the largest insulin-sensitive tissue in the body, is a major protein

reservoir and contributor to metabolic activity. When muscle wasting occurs, metabolic

dysfunction can follow, leaving the patient susceptible to not only developing insulin resistance

and Type 2 Diabetes, but also suffering from the long-term effects of muscle atrophy. Chemotherapy and radiation, while beneficial, also induce irreversible systemic effects through intracellular protein degradation and satellite cell damage, which promotes skeletal muscle atrophy in patients and decreased quality of life [9].

Metformin, a well-tolerated anti-diabetic medication, is widely used to improve overall glucose metabolism via regulation of hepatic gluconeogenesis through activation of adenosine monophosphate activated protein kinase (AMPK) [24, 25]. AMPK is a cellular energy sensor responsible for increasing insulin sensitivity, promoting glucose uptake, reducing hepatic glucose production, and leading to overall improved systemic glucose metabolism. While Metformin is used as a first measure of defense and prevention for Type 2 Diabetes, Metformin may be an attractive target to manage cancer-induced metabolic dysfunction and cachexia. Within skeletal muscle, Metformin delays satellite cell activation through preservation of the satellite cell pool in a lower metabolic state, sustaining quiescence [28]. Maintenance of the stem cell population is crucial to preserve skeletal muscle mass, repair, and function [29]. Metformin also increases peroxisome proliferator-activated receptor-coactivator-1α (PGC-1α) protein expression, a transcriptional co-activator involved in mitochondrial biogenesis, glucose metabolism, and muscle fiber type [30]. PGC-1α increases the expression of genes involved in energy metabolism, which is thought to protect skeletal muscle from atrophy, and suppresses Forkhead Box O3 (FoxO3), a transcription factor that induces the expression of ubiquitin-ligases involved in atrophy [31].

It is currently unknown how the combination of Metformin treatment and NSCLC directly influence skeletal muscle health and metabolism. The purpose of this study was to

investigate the effects of NSCLC tumor progression on skeletal muscle health and the role of

Metformin may play in attenuating any deleterious effects within skeletal muscle.

3.2 Experimental Design and Methods

3.2.1 Experimental Animals

Six week-old male (n=12) and female (n=12) C57BL/6j mice (Jackson Laboratory, Bar

Harbor, ME) were randomly assigned into a control group (lung cancer without Metformin

treatment) (n=12; 6 males, 6 females) and a Metformin treatment group (lung cancer with

Metformin treatment) (n=12; 6 males, 6 females). Control (n=7) and Metformin (n=9) animals

completed the study and were used in statistical calculations.

All mice were provided with *ad libitum* access to water and standard rodent chow

(Teklad Diets 2919, Envigo). Male and female C57BL/6 mice were used to address Metformin's

efficacy on reducing lung tumor burden in immunocompetent mice. We used the Lewis Lung

Carcinoma immunocompetent mouse model to mimic lung tumor development including the

immune system modulations. The non-small cell lung carcinoma (NSCLC) Lewis Lung

Carcinoma (LL/2) cells is syngeneic with C57BL/6 mice and stably and constitutively expresses

a luciferase reporter (Imanis Life Sciences). All aspects of this study were approved by the

Institutional Animal Care and Use Committee at the University of North Carolina at Charlotte.

3.2.2 Orthotopic Injection

Animal hairs were removed and the ventral and left thoracic regions were aseptically

prepared. Prior to receiving an LL/2 cancer injection, all animals were imaged and baseline

images acquired using the In Vivo Imaging System (IVIS). Under anesthesia (1-3% isoflurane),

mice received one orthotopic lung injection of LL/2 cells into the left lung. LL/2 cells (1.0×10^3)

were administered in PBS and Matrigel® (10μg; Dulbecco's Modified Eagle's Medium with

50ug/mL gentamycin Phenol Red Free, Corning). Matrigel® facilitated both tumor cell growth and homing within the lung tissue [66]. A small incision (3-5mm) was made to expose the area surrounding the seventh and eighth ribs. Cells were injected orthotopically into the lung using a sterile 29-gauge syringe and the incision was closed with a wound clip. Following surgery, all mice were individually housed and allowed to recover for one week. Animal weights were recorded weekly throughout the study. Any mice showing signs of distress or exceeding 20% body mass loss, in accordance with approved IACUC guidelines, were euthanized to maintain humane endpoints for all animals.

3.2.3 Metformin Treatment

Following tumor detection with the *In Vitro* Imaging System (IVIS), control and Metformin-treated mice were injected intraperitoneally (i.p.) with saline and Metformin (250mg/kg, twice weekly). Metformin Hydrochloride (1084; Sigma Aldrich) was dissolved in 1x phosphate buffered saline (PBS) and sterile filtered (0.2µm) for a final dose of 250mg/kg. Metformin was cultured on nutrient agar plates to ensure no visible contaminants were present. Metformin mice received 250mg/kg Metformin via intraperitoneal (i.p.) injection twice a week [39, 67]. Control mice received a placebo of 1x phosphate buffered saline (PBS) solution via an i.p. injection twice a week. 5-week post-tumor implantation, mice were euthanized (>4% isoflurane), and tissues collected, snap frozen on liquid nitrogen, and stored at -80°C.

3.2.4 Gastrocnemius Tissue Harvesting, Homogenization and mRNA Isolation

Upon sacrifice, the skeletal muscle tissue was harvested, and muscle weights were taken for the gastrocnemius muscle. Tissues were snap frozen over liquid nitrogen and stored at -80°C. The left gastrocnemius muscle was homogenized using ≤30mg of tissue in 300uL of buffer RLT supplemented with 1% β-mercaptoethanol. Tissue was disrupted with a bead blaster

homogenizer (BeadBlasterTM 24 Microtube, Sigma) with 2 separate rounds of 2-30 second intervals at 619 meters/second followed by 1 minute of rest. Following lysis, mRNA was extracted utilizing an RNeasy Fibrous Tissue kit (74704; Qiagen). Proteinase K and RNase-free water were added to each sample, allowed to incubate at 55° F for 10 minutes, and centrifuged at 10,000 x g for 3 minutes. Supernatnant was transferred to a clean tube. Following the addition of ethanol, the upper aqueous phase was removed and placed into a clean tube and washed multiple times. mRNA was eluted using RNAse-free water though an RNeasy column. The quality and quantity of mRNA was assessed using NanoDrop 1000. Briefly, 2uL of RNAse-free water was used to blank the NanoDrop and 2uL of sample was loaded onto the pedestal for quatnification. Quality of mRNA was determined using the 260/280 and 260/230 ratios.

3.2.5 cDNA and Real-time PCR

mRNA (1 µg of RNA/reaction) was reverse transcribed to cDNA using Applied Biosystems cDNA synthesis kit (4368814; Fisher Scientific). The quality of cDNA was assessed via spectrophotometry (NanoDrop 1000 Spectrophotometer, ThermoFisher). Samples of cDNA were diluted to 5ng/µl (20 µg/reaction) and Radiant™ Green Hi-ROX Green (QS2005; Alkali Scientific) was utilized for all real-time polymerase chain reaction (qPCR) and was performed on a Step One Plus system (Applied Biosystems). Quantitative real-time qPCR experiments assessed genes involved in skeletal muscle mass, metabolism and inflammation. Genes involved in inflammatory responses included F4/80 and tumor necrosis alpha (TNF-α). Phosphatase and tensin homolog (PTEN), an atrophy-associated gene, and peroxisome proliferator-activated receptor-γ coactivator 1 alpha (PGC-1α), an gene involved in skeletal muscle metabolism were also assessed. Glyceraldehyde 3-phosphate (GAPDH) was the housekeeping gene for all qPCR experiments. SYBR green ROX cycling): cDNA was activated at 95°C for 2 minutes followed

by 20 cycles of 95°C for 5 seconds (denaturation) and 60°C for 20 seconds (annealing/extension).

3.2.6 Gastrocnemius Tissue Protein Isolation and Quantification

Gastrocnemius tissue (≤30mg) was placed into a microcentrifuge tube with beads in cell lysis buffer (30µl/mg tissue) containing ice cold radioimmunoprecipitation assay (RIPA) buffer (sc-24948; Santa Cruz, supplemented with 10% sodium dodecyl sulfate (SDS), 1% Triton X-100, protease cocktail inhibitor. Tissue was disrupted with a bead blaster homogenizer (BeadBlasterTM 24 Microtube; Sigma) with 2 separate rounds of 2-30 second intervals at 619 meters/second (check this for with photo?) followed by 1 minute of rest. Samples were placed on ice for 5 minutes on ice between the 2 separate rounds. Following lysis, protein underwent centrifugation at 10,000 x g (rcf) for 10 minutes at 4°C. Protein supernatant was quantified using a Pierce BCA protein kit (23225; Thermo Fisher).

3.2.7 Western Blotting

Western blotting was used to assess proteins regulating skeletal muscle metabolism. Protein samples prepared in 1x loading buffer, supplemented with 10% β-mercaptoethanol, were denatured at 95°C for 3 minutes and then immediately placed on ice for 5 minutes. Protein samples (30µg/well) were loaded onto 10% SDS-page gels and were run at 225V for 40 minutes in 1x running buffer. Following electrophoresis, the gel was placed into 1x Towbin's transfer buffer, supplemented with 20% methanol, for 15 minutes. Proteins were transferred onto a 0.45µM Polyvinylidene difluoride (PVDF-FL) membrane at 100V for 90 minutes in 4°C. Following transfer, membranes were washed once in 1x Tris-buffered saline (TBS) for 5 minutes. Next the membrane underwent blocking in Odyssey Blocking Buffer and TBS (1:1) for 1 hour at room temp. After blocking, the primary antibodies were added overnight (16 hours).

Primary antibodies included: pAMPK, AMPK, STAT3, and REDD1 (Table 3.6.3). Following removal of the primary antibodies, the membrane underwent 3 x 5 minute washes in 1X Tris-buffered saline with Tween 20 (TBST). Secondary antibodies (1:10,0000 in TBST) were targeted to primary antibodies and incubated at room temp for 2 hours. Next, membranes were washed twice in 1x TBST and twice in 1x TBS. Membranes were imaged using the Odyssey® Licor CLx System. Using the same software, bands were quantified using arbitrary units as a measure of integrated optical density. Phosphorylation (pSTAT3) proteins were normalized to total (STAT3) protein expression. Total (STAT3, AMPK, REDD1) proteins were normalized to Glyceraldehyde 3-phosphate dehydrogenase (GAPDH).

3.2.8 Statistical Analyses

All treatments were run with an unpaired t-test, except where variances significantly differed ($p < 0.05$). In those cases, a Welch's t-test was used to compare differences in gene expression between treatment groups. Statistical significance was set at an *a priori* of $p \leq 0.05$. All statistical analyses and graphs were completed using GraphPad Prism (version 9.1). Gastrocnemius muscle masses are means ± SD. All other data are presented means ± SEM.

3.3 Results

3.3.1 Maintenance of Skeletal Muscle Mass

Skeletal muscle mass was maintained in all mice, irrespective of treatment (Table 3.6.1). Gastrocnemius muscle mass between Control (Left: 100.0 ± 20.0mg; Right: 102.0 ± 19.2mg) and Metformin (Left: 102.9 ± 17.4mg; Right: 97.5 ± 17.5mg) treated mice did not significantly differ (Left: $p = 0.0800$; Right: $p = 0.672$).

3.3.2 Gastrocnemius Gene Expression

Genes involved in maintaining skeletal muscle mass and inflammatory signaling were not significantly different with regard to treatment (Figure 3.5.1). Metformin did not alter skeletal muscle PGC1-α mRNA (p=0.816), MAFBx mRNA levels (p=0.325), TNF-α mRNA levels (p=0.111) or F480 mRNA levels (p=0.076) expression. Two outliers were removed from PGC1-α mRNA expression data. Separation via treatment and sex revealed no significant differences in gene expression.

3.3.2 Gastrocnemius Protein Expression

Skeletal muscle proteins that promote atrophy and regulate metabolism did not reveal detectable differences between control and Metformin treated groups (pSTAT3, p=0.5889; STAT3, p=0.6534; REDD1, p=0.6998; AMPK, p=0.6387).

3.4 Discussion and Conclusion

The present study aimed to assess the effects of Metformin in support of skeletal muscle health during LL/2 tumor progression in C57BL/6 mice. The data obtained highlight that the regimen used (250 mg/kg, twice weekly, IP) in an immunocompetent model of NSCLC was not associated with significant improvement in skeletal muscle health.

Key skeletal muscle markers of muscle metabolism (PGC1-α 1) and atrophy (MAFbx) were chosen to assesses overall skeletal muscle health, but exhibited no marked differences in gene expression. However, separating expression based off sex reveals some variation within each treatment, suggesting a potential source of noise evidenced in graphs grouped by treatment (Figure 3.5.1). PGC1-α 1 is a transcriptional co-activator critical for regulating energy metabolism and mitochondrial biogenesis [88]. Higher expression of PGC1-α suppresses atrophy-associated genes (Muscle RING finger 1 and muscle atrophy F-box (MAFbx)/atrogin-1) and lower expressions of PGC1-α can be concomitant with rapid muscle atrophy, such as cancer

cachexia [31]. Metformin has also been previously shown to increase levels of PGC1-α in skeletal muscle via AMPK phosphorylation [30]. Neither MAFbx nor PGC1-α showed any marked changes during NSCLC cancer development nor in response to Metformin treatment, suggesting that conditions in this study were not significant enough to induce rapid atrophy (<6 weeks).

Body mass and gastrocnemius muscle mass were also maintained, indicating that weight loss was probably not an indicative marker of cancer-induced cachexia. Cross-sectional area analyses of harvested tissues would have provided a clearer picture of the presence or absence of skeletal muscle atrophy, potentially propitiated via NSCLC development in the animals, but significant freezer damage to these tissues precluded these analyses. Since muscle mass was not significantly affected in this immunocompetent model of LL/2, it is highly probably that the balance between protein synthesis and degradation was likely maintained, suggesting that a cancer induced cachexia may not have been achieved in this study. It is also possible the endpoint of this study preceded the development cachexia.

Although no significant differences gene expression markers nor any correlation between tumor burden or inflammatory markers were detected, it is possible that a modest inflammatory response was occurring within skeletal muscle. Metformin treated mice showed elevated gene expression levels of inflammatory markers, namely macrophage infiltration (F4/80) and inflammatory cytokine (TNF-α) were elevated, but not significantly. Importantly, infiltration of pro-inflammatory macrophages (including F4/80) has been shown to be a distinct characteristic that is linked to obese, insulin resistant, and cancer cachexia populations [89-91]. Low-grade inflammation coincides with the onset of insulin resistance, which can be indicative of repressed skeletal muscle health and reduced glucose disposal. Elevated TNF-α levels are also associated

with increased catabolic activity in skeletal muscle, such as protein degradation, insulin resistance, impaired myogenesis and contractile dysfunction [92, 93].

Signal transducer and activator of transcription 3 (STAT3), a cytokine transcription factor, has been linked with systemic inflammation in cancer cachexia [94]. Importantly STAT3 is a critical regulator of satellite cell self-renewal and STAT3 signaling plays an important role in muscle wasting, including cachexia [95]. Findings from this present study revealed no phosphorylation of pSTAT3 Ser727 or change in total STAT3 protein expression, suggesting that skeletal muscle wasting, if present, was not detected through this signaling pathway. Because the orthoptoic injection mimics the tumor development at the lungs, it is possible that a longer timeline or the combination of treatment modalities with irradiation or chemotherapeutics would better mimic the onset of muscle wasting.

Literature also shows a Lewis lung carcinoma mouse model attenuating expression of fundamental genes involved in the phosphatidylinositol 3-kinase (PI3K)-protein kinase B (Akt) pathway [52]. The PI3K/AKT pathway, which is often constitutively active in tumor cells, plays an important role in cellular proliferation, growth, metabolism, and protein synthesis [53]. Reduced expression of regulatory genes in the PI3K/AKT pathway could lead to mitochondrial dysfunction and skeletal muscle wasting [52]. Importantly, Metformin treatment in tumor bearing rats decreases skeletal muscle wasting and improves protein metabolism, attenuating cancer-induced cachexia [54]. Regulated in development and DNA damage response (REDD1) is a ubiquitous protein that is well-known endogenous inhibitor the AKT/mTOR pathway [96]. Not surprisingly, this means that REDD1 does play a role in regulating cell growth, mitochondrial function, oxidative stress, and apoptosis [97]. Recent studies highlight the importance of REDD1 in maintaining skeletal muscle mass [98]. The present study revealed no

differences in REDD1 expression in control or Metformin treated animals. In contrast, a murine model of Lewis Lung Carcinoma shows skeletal muscle mass loss between 28-35 days post-tumor concomitant with increased that REDD1 gene expression in collected tissues. The increased REDD1 expression was associated with a lower mTOR expression, suggesting that REDD1 may be associated with curbing mTOR signaling during later stages of cachexia development [99]. It is important to note, however, these animals received the LL/2 injection directly into the flank rather than orthotopically into the lung, marking differences in the overall development of skeletal muscle wasting. It is probable that the differences seen in the literature with REDD1 expression compared to the findings in the present study are likely attributed to the variation in delivery of lung cancers cells to the respective animals.

Although other AKT markers were not included in the present study, assessing these markers in future models could provide insight into the potential influence of Metformin supporting skeletal muscle health in a Lewis Lung carcinoma mouse model. Using a model with respect to an orthotopic delivery of lung cancer cells to the lungs rather than directly into the flank of animals does provide a valuable perspective as lung cancer does originate within lung tissue. Futures studies should consider including more frequent Metformin dosing in combination with standard chemotherapeutics known to induce deleterious effects to skeletal muscle.

3.5 Figures

A)

B)

C)

D)
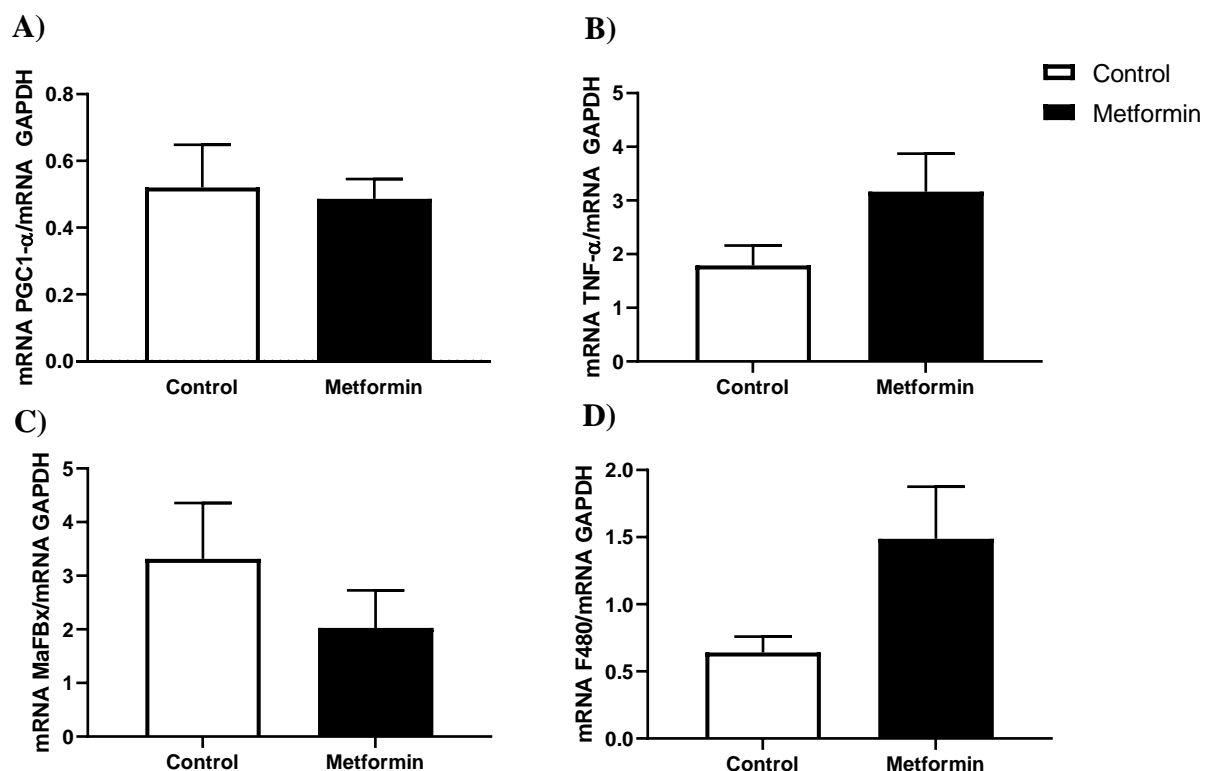
Figure 3.5.1. Gene expression in gastrocnemius muscle from C57BL/6 mice with Non-Small Cell Lung Cancer. A) mRNA Peroxisome proliferator-activated receptor-gamma coactivator-1alpha (PGC1-α)/GAPDH; B) mRNA tumor necrosis factor-alpha (TNF-α)/GAPDH; C) mRNA muscle atrophy F-box (MAFbx)/GAPDH; D) mRNA F480/GAPDH. Gastrocnemius mRNA expression from C57BL/6 mice with NSCLC concomitant with or without Metformin (250mg/kg) treatment. Data were analyzed using an unpaired t-test. Sample size: Control, n=7; Metformin, n=7. Data are mean ± SEM.
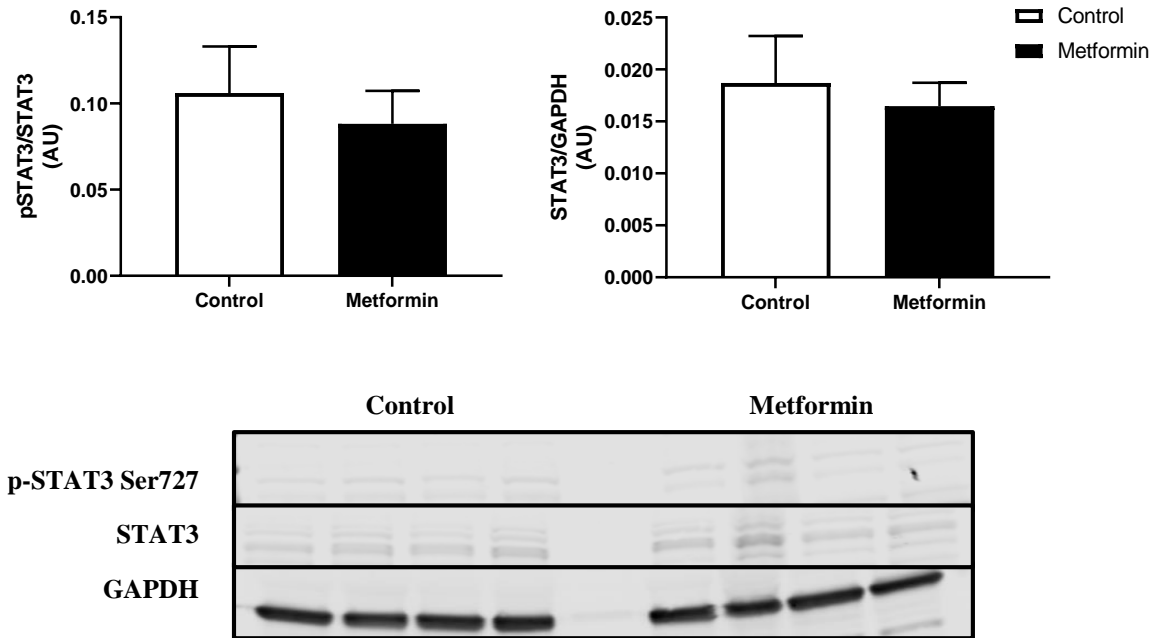
Figure 3.5.2. STAT3 expression in gastrocnemius muscle from C57BL/6 mice with Non-Small Cell Lung Cancer. Phospho (p)- Signal transducer and activator of transcription 3 (STAT3) Ser727/Total STAT3 and STAT3/GAPDH expression (Arbitrary Units, AU) in gastrocnemius muscle from C57BL/6 mice with NSCLC concomitant with or without Metformin (250mg/kg) treatment. Data were analyzed using an unpaired t-test. Sample size: Control, n=7; Metformin, n=8. Data are mean ± SEM.
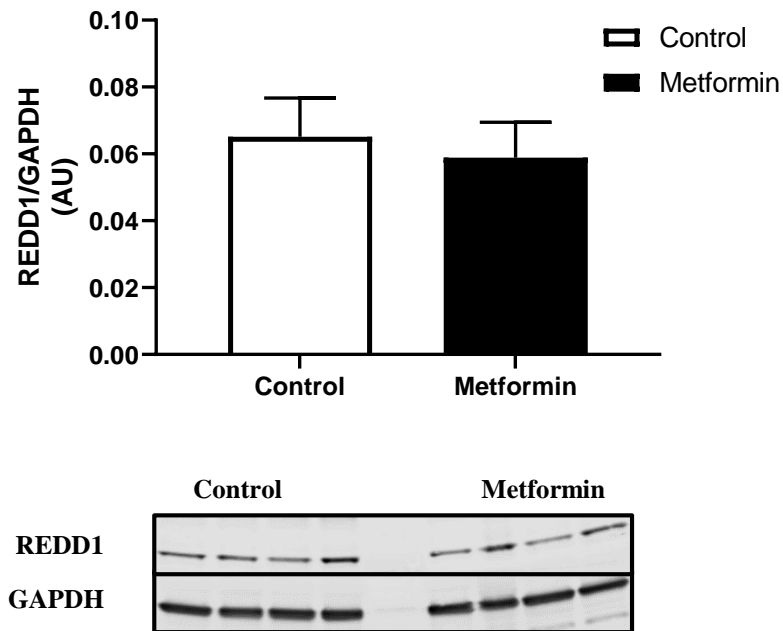
Figure 3.5.3. REDD1 expression in gastrocnemius muscle from C57BL/6 mice with Non-Small Cell Lung Cancer. Regulated in development and DNA damage responses 1 (REDD1)/GAPDH expression (Arbitrary Units, AU) in gastrocnemius muscle from C57BL/6 mice with NSCLC concomitant with or without Metformin (250mg/kg) treatment. Data were analyzed using an unpaired t-test. Sample size: Control, n=7; Metformin, n=8. Data are mean ± SEM.
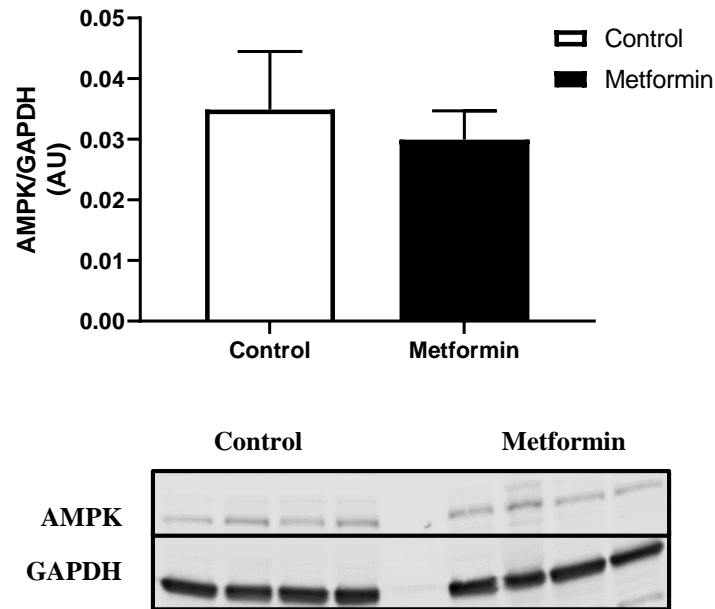
Figure 3.5.4. AMPK expression in gastrocnemius muscle from C57BL/6 mice with Non-Small Cell Lung Cancer. Total adenosine monophosphate-activated protein kinase (AMPK)/GAPDH expression (Arbitrary Units, AU) in gastrocnemius muscle from C57BL/6 mice with NSCLC concomitant with or without Metformin (250mg/kg) treatment. Data were analyzed using an unpaired t-test. Sample size: Control, n=7; Metformin, n=8. Data are mean ± SEM.

3.6 Tables

Table 3.6.1. Gastrocnemius Muscle Mass in C57BL/6 mice with Non-Small Cell Lung Cancer.

	Left Gastrocnemius (mg)	Right Gastrocnemius (mg)
Control	100.0 ± 20.0	102.0 ± 19.2
Metformin	102.9 ± 17.4	97.5 ± 17.5

*Data are mean $\pm$ SD. Mg: milligrams

Table 3.6.2 Primers used for Gene Expression Analyses.

Primer		Sequence
TNF-α	Forward	CCAGACCCTCACACTCAGATC
	Reverse	CACTTGGTGGTTTGCTACGAC
F4/80	Forward	CTTTGGCTATGGGCTTCCAGTC
	Reverse	GCAAGGAGGACAGAGTTTATCGTG
PGC-1α	Forward	TGATGTGAATGACTTGGATACAGACA
	Reverse	GCTCATTGTTGTACTGGTTGGATATG
MAFbx	Forward	CCAGGATCCGCAGCCCTCCA
	Reverse	ATGCGGCGCGTTGGGAAGAT
GAPDH	Forward	ATGTTTGTGATGGGTGTGAA
	Reverse	ATGCCAAAGTTGTCATGGAT

TNF-α: Tumor necrosis factor alpha; PGC-1α: Peroxisome proliferator-activated receptor-γ coactivator 1 alpha; MAFbx: muscle-specific ubiquitin ligases muscle atrophy F-box; GAPDH: Glyceraldehyde 3-phosphate dehydrogenase

Table 3.6.3 Primary Antibodies used for Western Blot Analyses.

Antibody	Catalog #, Company	Dilution
Phospho AMPK Thr 172	(#4188; CS)	1: 500
AMPK	(#2532; CS)	1: 500
P-STAT3 Ser727	(#9134; CS)	1: 500
Total STAT3	(#4904, CS)	1: 500
REDD1	(#PIPA520495; FS)	1:1000
GAPDH	(#MAB374; CS)	1:5000

AMPK: 5' Adenosine Monophosphate-Activated Protein Kinase; Ser: Serine; STAT3: Signal transducer and activator transcription 3; Thr: Threonine; REDD1: Regulated in development and DNA damage responses; GAPDH: Glyceraldehyde 3-phosphate dehydrogenase; CS: Cell signaling; FS: FisherScientific

CHAPTER 4: EFFECTS OF METFORMIN TREATMENT ON *IN VITRO* LL/2 TUMOR

GROWTH

4.1 Introduction

Metformin, a commonly used and well-tolerated Type 2 Diabetic drug, is a widely used

to promote glucose uptake, increase insulin sensitivity, and improve systemic glucose

metabolism [24, 25]. Metformin primarily acts through an activating adenosine monophosphate

(AMPK) activated protein kinase (AMPK). AMPK is an important cellular energy sensor that

promotes insulin sensitivity in peripheral tissues and reduced adipocyte formation [24].

Importantly, Metformin elicits anti-tumorigenic effects in many cancers, including prostate,

colon, breast, skin, and obesity-activated thyroid cancer [32-36]. In cancers, Metformin induces

alterations in cellular proliferation, apoptosis, cell cycle progression, and inflammatory responses

through signaling pathways such including AMPK, mechanistic target of rapamycin (mTOR),

mitogen activated protein kinase (MAPK), and the nuclear factor kappa-light-chain-enhancer of

activated B cells (NFkB) and signal transducer and activator of transcription 3 (STAT3) pathway

[37-40].

Because Metformin canonically inhibits the electron transport chain, a large portion of

cancer studies demonstrate Metformin's anti-cancer action via AMPK- dependent mechanisms.

When mitochondrial function is impaired, liver kinase B 1 (LKB1) phosphorylates Threonine

172, activating AMPK [43]. LKB-1-activation of AMPK phosphorylates and activates Tumor

sclerosis complex 1 and 2 (TSC 1/2) leading to a negative regulation of mTOR activity, reducing

cell growth and proliferation [44]. Activated AMPK also induces cell cycle arrest through

activation of protein 53 (p53), leading to upregulation of pro-apoptotic genes [45, 46].

Metformin has also been shown to combat tumorigenesis independently of AMPK through reduced insulin like growth factor (IGF-1), leading to phosphatidylinositol-3,4,5-triphosphate (PIP3) recruitment and subsequent activation of Protein Kinase B/AKT [1, 48]. AKT phosphorylates TSC1/2, rendering TSC1/2 inactive and hindering mTOR activity [49]. Specifically in a Lewis lung carcinoma mouse model, fundamental genes involved in the phosphatidylinositol 3-kinase (PI3K)-protein kinase B (Akt) pathway were attenuated [52]. The PI3K/AKT pathway, which is often constitutively active in tumor cells, plays an important role in cellular proliferation, growth, metabolism, and protein synthesis [53]. Reduced expression of regulatory genes in the PI3K/AKT pathway could lead to mitochondrial dysfunction [52].

Notch signaling is well-conserved transmembrane cellular signaling pathway particularly important for determining cell fate, both during development and in maintaining homeostasis of adult tissues [100]. Notch is a ligand-dependent intercellular pathway regulating cellular differentiation, proliferation, and apoptosis. Activation of Notch signaling occurs when ubiquitinated ligands (jagged proteins or delta like proteins) initiate a cleavage cascade via metalloproteases and γ-secretases, releasing the Notch intracellular domain (NCID) from the transmembrane domain [101]. When NCID is released into the cytosol, it translocates into the nucleus, resulting in transcription of target genes, including hair and enhancer of split 1 (HES1). Alterations in Notch signaling, particularly over activation, are prevalent in many diseases, including cancer [102]. Over activation of Notch signaling drives Non-Small Cell Lung Cancer (NSCLC) tumorigenesis [103]. In NSCLC, many studies have also found mutations within Notch signaling cascade [104].

The AMPK-independent action of Metformin on NSCLC progression remains largely uncharacterized, which may be due to Metformin's primary role as an AMPK activator. While

Metformin demonstrates antineoplastic effects via cell cycle arrest, the mechanism underlying this pharmaceutical's action on NSCLC tumor development still require elucidation. The purpose of this study was to better understand the oncogenic programming alternations Metformin elicits on NSCLC cell proliferation.

4.2 Experimental Design and Methods

4.2.1 Cell Culture

Non-small cell lung cancer (NSCLC) cells (Cl050; Imanis Life Sciences) were grown in standard growth media with 10% fetal bovine serum and 1% penicillin-streptomycin. Cells were passaged in 2μg/ml puromycin to maintain high luciferase fluorescence and cell passages two and six were utilized for all experiments. Cells were maintained at 37°C for 48 hours or until predetermined time points.

4.2.2. Metformin Treatment

NSCLC cells were seeded at a density of 30,000 cells/well and allowed to proliferate for 24 hours (~30% confluence). Cells were treated with varying isovolumetric concentrations (5mM-15mM) of Metformin Hydrochloride (PHR1084; Sigma) for pre-determined time points to assess the optimal treatment concentration.

4.2.3 Gamma Secretase Inhibition

NSCLC were seeded at a density of 15,000 cells/well and allowed to proliferate for 24 hours (~30% confluence). A gamma secretase inhibitor (565771; Sigma) was added to each well at a final concentration of 4uM GSI/well (control cells received equal volume DMSO) every 12 hours for 48 hours. Cells were collected for both mRNA analyses and immunocytochemistry.

4.2.4 Co-treatment with Metformin and Gamma Secretase Inhibition

NSCLC were seeded at a density of 15,000 cells/well and allowed to proliferate for 24 hours (~30% confluence). A gamma secretase inhibitor (565771; Sigma) was added to each well at a final concentration of 4uM GSI/well (control cells received equal volume DMSO) every 12 hours for 48 hours. Metformin Hydrochloride was added to wells at a final of 10mM Metformin/well. Cells were analyzed via immunofluorescence.

4.2.5 MTT Assay

NSCLC cells were grown for 24 hours (~30% confluence) and serum-starved overnight with serum-free media to induce quiescence. Cells were treated with equal volumes of fresh growth media followed by Metformin treatment with a range of concentrations from 5mm to 15mM. NSCLC cell viability was assessed every 24 hours for 3 days via an MTT assay using 3-(4,5-Dimethyltiazol-2-yl)-2,5-Diphenyltetrazolium Bromide (MTT) reagent (M2128; Sigma). MTT reagent was added to wells at a final concentration of 1mg/ml 4 hours prior to the collection time point, allowing for the formation of blue formazan crystals in growing cells. Crystals were dissolved with dimethyl sulfoxide (DMSO, D8418; Sigma). Absorbance was measured at 560nm.

4.2.6 Cell Lysate Homogenization and mRNA Quantification

mRNA was extracted utilizing a GeneJET RNA purification kit (K0731; ThermoFisher Scientific). Briefly, growth media was removed from adherent cells, cells were washed with 1x PBS, and removed from the culture plate by scraping in 50µl 1x PBS. Cells were transferred to a microcentrifuge tube and centrifuged for 5 minutes at 250 x g. Supernatant was removed and cells were resuspended in lysis buffer supplemented with 2% β-mercaptoethanol and gently vortexed for 10 seconds. 360µl of ethanol (96-100%) was added to precipitate the mRNA. The cell lysate was transferred to a GeneJET purification column and centrifuged for 1 minute at

12,000 x g. After all lysate was filtered through the column, 700µl of Wash Buffer 1

(supplemented with 20% ethanol) was added to the column and centrifuged for 1 minute at

12,000 x g. Next, 600µl of Wash Buffer 2 (supplemented with 63% ethanol) was added to the

column and centrifuged for 1 minute at 12,000 x g. 250µL of Wash Buffer 2 was added to the

purification column and centrifuged for another 2 minutes at 12,000 x g. mRNA from was eluted

using RNAse-free water though an RNeasy column. The quality and quantity of mRNA was

assessed using NanoDrop 1000. Briefly, 2uL of RNAse-free water was used to blank the

NanoDrop. 2uL of sample was loaded onto the pedestal and quantified. Quality of mRNA was

determined using the 260/280 and 260/230 ratios.

4.2.7 cDNA and Real-time PCR

mRNA (1 µg of RNA/reaction) was reverse transcribed to cDNA using Applied

Biosystems cDNA synthesis kit (4368814; Fisher Scientific). The quality of cDNA was assessed

via spectrophotometry (NanoDrop 1000 Spectrophotometer, ThermoFisher). Samples of cDNA

were diluted to 5ng/µl (20 µg/reaction) and Radiant™ Green Hi-ROX Green (QS2005; Alkali

Scientific) was utilized for all real-time polymerase chain reaction (qPCR) and was performed on

a Step One Plus system (Applied Biosystems). cDNA was activated at 95°C for 2 minutes

followed by 20 cycles of 95°C for 5 seconds (denaturation) and 60°C for 20 seconds

(annealing/extension). Quantitative real-time qPCR experiments assessed genes involved in cell

cycle regulation and pro-apoptotic markers including, Cyclin D, cyclin dependent kinase 4

(CDK4), protein 27 (p27), protein 21 (p21), and Hairy and Enhancer of Split 1 (Hes1) (Table

4.6.1). Glyceraldehyde 3-phosphate (GAPDH) was the housekeeping gene for all qPCR

experiments.

4.2.8 Western Blotting

Western blotting was used to assess proteins regulating cell growth and metabolism. Protein samples prepared in 1x loading buffer, supplemented with 10% β-mercaptoethanol, were denatured at 95°C for 3 minutes and then immediately placed on ice for 5 minutes. Protein samples (30μg/well) were loaded onto 8% or 10% SDS-page gels and were run at 225V for 40 minutes for 8% gels and 43 minutes for 10% gels in 1x running buffer. Following electrophoresis, the gel was placed into 1x Towbin's transfer buffer, supplemented with 20% methanol, for 15 minutes. Proteins were transferred onto a 0.45μM Polyvinylidene difluoride (PVDF-FL) membrane at 100V for 90 minutes in 4°C. Following transfer, membranes were washed once in 1x Tris-buffered saline (TBS) for 5 minutes. Next the membrane underwent blocking in Odyssey Blocking Buffer and TBS (1:1) for 1 hour at room temp. After blocking, the primary antibodies were added overnight (16 hours). Primary antibodies included: mammalian target of rapamycin (mTOR), regulated in development and DNA damage responses 1 (REDD1), 5' Adenosine monophosphate-activated protein kinase (AMPK), Protein Kinase B (PKB/AKT), tumor suppression include protein 53 (p53) and Signal transducer and activator transcription 3 (STAT3) (Table 4.6.2). Following removal of the primary antibodies, the membrane underwent 3 x 5 minute washes in 1X Tris-buffered saline with Tween 20 (TBST). Secondary antibodies (1:10,0000 in TBST) were targeted to primary antibodies and incubated at room temp for 2 hours. Next, membranes were washed twice in 1x TBST and twice in 1x TBS. Membranes were imaged using the Odyssey® Licor CLx System. Using the same software, bands were quantified using arbitrary units as a measure of integrated optical density. Phosphorylation (pSTAT3, pAKT, pmTOR, pAMPK, p-p53) proteins were normalized to total (STAT3, AKT, mTOR, AMPK, p53) protein expression. Total (STAT3, AKT, mTOR, AMPK, REDD1, p53) proteins were normalized to Glyceraldehyde 3-phosphate dehydrogenase (GAPDH).

4.2.9 Immunofluorescence Staining

Following 48 hours of treatment, cells were washed two times with 1x PBS. Cells were fixed in cold mixture of 70% ethanol and 30% acetone for 10 minutes at room temperature. Cells were washed two times with 1x PBS. Cells were permeabilized with 0.05% Triton X-100 in 10 minutes at room temperature. Following another two rounds of washes with 1x PBS, cells underwent blocking with an immunohistochemistry (IHC) blocking buffer for 30 minutes at room temperature. Next, cells were incubated with a primary antibody for Ki-67 (9129; Cell Signaling) diluted in IHC blocking buffer at room temperature for two hours. Cells were washed three times with 1x PBS. Cells were incubated with a AlexaFluo 488 goat-anti-rabbit IgG secondary antibody (A11008; ThermoFisher) for 30 minutes at room temperature (Table 4.6.3). All cells were washed three more times with 1x PBS. Cells were mounted using 4',6-diamidino-2-phenylindole (DAPI) Fluoromont-G$^®$ (0100-20; SouthernBiotech) and a coverslip.

4.2.10 Immunofluorescence Quantification

Immunofluorescence images were captured using a IX71 inverted fluorescence microscope (Olympus^{TM}). Six images per well were captured using a consistent scanning pattern for every well. Separate images were taken for DAPI (International Standards Organization (ISO): 200; Exposure 32.05 milliseconds) and Ki-67 (ISO: 400; Exposure: 57.87 milliseconds) at their respective wavelength. Background was subtracted (contrast=8) for all images prior to merging. Co-localization of Ki-67 in nuclei was quantified using FIJI (Binary Feature Extractor). Briefly, merged images were split and brightness and threshold settings were consistent between images for both nuclei detection and sufficient dissection of clustered nuclei. The watershed feature was applied and the Biovoxxel plugin was used to extract binary features (Objects: DAPI; Selectors; Ki-67).

4.2.11 Statistical Analyses

A two-way ANOVA (time x treatment) was run to detect differences in NSCLC growth following treatment with varying concentrations of Metformin (5mm-15mM). A Tukey's post-hoc test was used to further detect differences. All treatments were run with an unpaired t-test, except where variances significantly differed ($p < 0.05$). In those cases, a Welch's t-test was used to compare differences in gene expression between treatment groups. Statistical significance was set at an *a priori* alpha value of $p \leq 0.05$. All statistical analyses and graphs were completed using GraphPad Prism (version 9.1). Data are presented means ± SEM.

4.3 Results

4.3.1 Proliferation of NSCLC cells following Metformin Treatment over 48 hours

There were significant fold changes in NSCLC proliferation with respect to both time [$F(2, 72) = 87.69$, *p < 0.0001*] and treatment [$F(5, 72) = 2.364$, *p=0.0482*]. Tukey's post-hoc test revealed that control cells underwent significantly increased growth over 48 hours (p <0.0001). After 48 hours, Metformin treatment (10mM-15mM) reduced proliferation of NSCLC cells compared to control cells (10mM Metformin, p=0.0094; 12.5mM Metformin, p=0.0015; 15mM Metformin, p=0.0018) (Figure 4.3.1).

4.3.2 *In Vitro* Gene Expression after 48 hour Metformin Treatment

10mM Metformin treatment for 48 hours did not significantly reduce gene expression in cell cycle regulators, namely Cyclin D (p=0.166), CDK 4 (p=0.059), P27 (p=0.422), and P21 (p=0.125). Treatment with Metformin (10mM) did significantly reduced HES1 expression (p=0.011) (Figure 4.5.2).

4.3.3 *In Vitro* Protein Expression following 48 hour Metformin Treatment

There were significant reductions in p-mTOR Ser2448 protein expression when compared to Metformin treated cells (p=0.003). Total mTOR protein expression remained the same, irrespective of treatment (p=0.134) (Figure 4.5.3). LL/2 cells without Metformin treatment showed significant reductions in p-p53 protein expression (p=0.0367), but Metformin treated cells exhibited reduced total p53 protein expression (p=0.0078) (Figure 4.5.4). Findings revealed no significant reductions in p-AMPK Thr172 (p=0.2390) or total AMPK (p=0.0730) protein expression (Figure 4.5.5). Both control and Metformin treated cells revealed similar p-STAT3 Ser727 (p=0.5291) and total STAT3 (p=0.4274) protein expression (Figure 4.5.6). Metformin treatment significantly decreased REDD1 protein expression in Metformin treated cells (p=0.0082) (Figure 4.5.7). There were no marked differences (p=0.0082) in total AKT protein expression (Figure 4.5.8).

4.3.4 Ki-67 Immunofluorescence following 48 hour Metformin Treatment

10mM Metformin treatment for 48 hours significantly reduced Ki-67 expression by ~65% over 48 hours (p=0.0021). The total number of nuclei was significantly reduced after treatment with 10mM Metformin (p=0.0020). The percent of extracted Ki-67 did not differ between treatments (p=0.4671) (Figure 4.3.10). Representative images were taken at 10x (Figure 4.3.10).

4.3.5 Ki-67 Immunofluorescence after 48 hour GSI Treatment

Ɣ-secretase inhibitor (GSI) treatment (4μM) significantly reduced Ki-67 expression by ~20% over 48 hours (p=0.0028). The total number of nuclei (p=0.2716) and Ki-67 extracted (p=0.6473) were not significantly different with Ɣ-secretase inhibition (Figure 4.3.11). Representative images were taken at 10x (Figure 4.3.11).

4.3.6 Ki-67 Immunofluorescence following 48 hour Co-treatment with GSI and Metformin

Co-treatment with 4µM GSI and 10mM Metformin significantly reduced Ki-67 expression by more than 50% over 48 hours (p=0.0245). The total number of nuclei was significantly reduced after co-treatment with 10mM Metformin and 4µM GSI for 48 hours (p=0.0191). The percent of extracted Ki-67 did not differ between treatments (p=0.1969) (Figure 4.3.12). Representative images were taken at 10x (Figure 4.3.12).

4.4 Discussion and Conclusion

The present study aimed to assess the effects of Metformin on LL/2 growth *in vitro*. These findings indicate that 48-hour treatment with Metformin (≥10mM) effectively decreases NSCLC growth *in vitro*, evidenced by decreased proliferation. Our findings are supported by previous literature showing that Metformin (5µM-20mM) does decrease NSCLC cancer cell proliferation [105, 106]. Lower doses of Metformin (5µM-5mM) have been show to inhibit human NSCLC cell proliferation *in vitro*, in a dose dependent manner [106]. However, the data obtained highlighted that concentrations below 10mM did not reduce proliferation when compared to control over 48 hours of treatment, suggesting that 10mM Metformin was the lowest, effective does to combat progression of this Lewis Lung Cancer cell line. It is probably that the differences seen could be cell line dependent as many of these previous studies used human cell lines, but the present study used a cell line sharing a genetic background with a C57BL/6 mouse. While using a lower concentration would have mirrored pharmacological dosing seen in the clinical population, these concentrations *in vitro* were not sufficient in this model. This poses a challenge in translatability to human therapy, as higher doses (1-50mM *in vitro*) lead to concentrations that are not safely achievable or relevant to the clinical population [71, 106].

Despite significantly reduced proliferation, marked changes in key tumor cell division: namely, cell cycle regulatory (p27, p21, CDK4, Cyclin D) gene expression within the tumor were not significantly altered through this treatment regimen. These markers were chosen because p27 and p21 can act as tumor suppressors and inhibit cell cycle progression [107-109]. CDK4 and Cyclin D are key players controlling regulation of the G1-S checkpoint and often undergo dysregulation in cancer cells [110]. Previous studies show that human lung cancer cell lines treated with Metformin (10-40mM) do undergo anti-neoplastic effects, evidenced by repressing cell growth and cell cycle regulatory proteins, namely p27, p57, and PTEN [111]. Metformin (20mM) induces cell cycle arrest, reduced proliferation, but not apoptosis in ovarian cancer cell lines [112]. Breast cancer cells do show increased p27 expression when treated with Metformin (10mM) for 48 hours [36]. However, most of these effects again were noted in response to much higher doses of Metformin treatment (≥10mM) *in vitro*.

While no marked changes were detected in these cell cycle regulatory genes, HES1 showed significant reductions in response to Metformin treatment (10mM). Because HES1 expression decreased when LL/2 cells were treated with Metformin, it was possible that NSCLC growth could have been, at least partially, mediated through Notch signaling, which is a transcriptional activator of HES1. To date, it does not appear that published studies highlight Metformin's efficacy on NSCLC cell lines and HES1 expression. However, a study on colorectal cancer patients with co-morbid Type 2 Diabetes do have abnormal cellular proliferation, which was correlated with Notch1/HES1 signaling being over activate and curbed with Metformin treatment [113]. Notch1 has been shown to be a potential independent prognostic factor for Small Cell Lung Carcinoma patients, within a small cohort having a high expression of Notch-1 (n=10) [114]. In addition to its role in cell cycle regulation, cellular growth, and survival, HES1

is also regulated through other pathways besides Notch (ie, Wnt and Hedgehog signaling pathways) and is a key player in T cell development [115]. It is possible that Metformin may be an effective pharmaceutical to better target cancers through HES1 signaling; however, much surrounding this potential mechanism of action still requires further study.

As an AMPK activator, Metformin would be expected to act along it's canonical mechanism of action, resulting in slowed grow through LKB-1 activation of AMPK [43] . Activated AMPK also induces cell cycle arrest through activation of protein 53 (p53), leading to upregulation of pro-apoptotic genes [45, 46]. However, the present findings revealed no detectable differences in p-AMPK or total AMPK protein expression in LL/2 cells treated with Metformin (10mM) for 48 hours. However, alterations in p53 were present. Specifically, reduced phosphorylation was present in control cells, while total p53 protein expression was increased in Metformin treated cells. Previous studies have shown Metformin (20mM) induced alterations in metabolism, including AMPK and glycolysis in ovarian cancer cell lines [112]. Further studies combining Metformin treatment (4-16mM) with low dose celecoxib (an anti-inflammatory drug, 4-16μM) show staunch reduction in NSCLC cell migration, invasions, and increased expression of p53, resulting in cell cycle arrest [116]. In breast cancer cells, AMPK has also been shown to activate forkhead transcription factors (FOXO), a protein family which can act a tumor suppressor through promotion of cell cycle arrest, DNA damage repair, and apoptosis [36]. Metformin does elicit tumor suppressing properties, particularly via p53 in this LL/2 cell line, however, other published studies better support the activation of AMPK via Metformin and downstream repression of tumor growth.

Literature shows a Lewis lung carcinoma mouse model attenuating expression of fundamental genes involved in the phosphatidylinositol 3-kinase (PI3K)-protein kinase B (Akt)

pathway [52]. The PI3K/AKT pathway plays an important role in cellular proliferation, growth, metabolism, and protein synthesis and is often constitutively active in tumor cells [53]. Regulated in development and DNA damage response (REDD1) is a ubiquitous protein that is well-known endogenous inhibitor the AKT/mTOR pathway [96]. Not surprisingly, this means that REDD1 does play a role in regulating cell growth, mitochondrial function, oxidative stress, and apoptosis [97]. In the present study, Metformin treatment (10mM) significantly reduced REDD1 expression in LL/2 cells, but overall AKT expression remained similar between both control and Metformin treated cells. If REDD1 were inhibiting mTOR activity, expression would be expected to increase following Metformin treatment. In contrast to the present study, REDD1 expression inhibits NSCLC invasiveness in human cell lines via mTOR suppression [117]. Prostate cancer cells treated with Metformin show increased expression of REDD1, promoting mTOR inhibition and cell cycle arrest [47]. In light of these contradictory findings, it does not appear that REDD1 plays a role in tumor suppression in this cell line, as it does not align with published findings. To better understand the role of REDD1 negatively regulating mTOR activity, it would be beneficial to assess REDD1 expression with LL/2 cells undergoing a co-treatment (ie, mTOR inhibitor or chemotherapeutic) with Metformin.

The findings from the current study also revealed noticeable reductions in phosphorylation of mTOR Ser2448, but not total mTOR protein, in control NSCLC cells. These findings are partially supported by another study of lung cancer cells exposed to Metformin over 72 hours [118]. Metformin treatment (10mM), particularly in combination with rapamycin (an inhibitor of mTOR), reduced the viability of human lung cancer cell that were resistant to cisplatin [118]. Proteomic analyses revealed that these anti-proliferative effects were associated

with mTOR signaling [118]. In order for Metformin to be more effective, co-treatment was necessary to promote the most anti-proliferative effect in lung cancer cells.

STAT3 also plays a critical role, not only in signal transduction, but also through cancer-promoting inflammation and increasing anti-tumor immunity [119]. In human NSCLC, Metformin targets STAT3, curbing tumor proliferation [120], but findings from the present study revealed no change in phosphorylation or total STAT3 expression. This was a surprising finding as STAT3 is often upregulated in many cancers. In particular, Metformin inhibits cell growth, through targeting STAT3, in triple negative breast cancers [121]. Normally these cancers show upregulation of STAT3 and phosphorylation of STAT3 at Tyr705 and Ser727, but are partially sensitive to Metformin, promoting a strong growth inhibitory and apoptotic effect in these cells [121]. In addition to breast cancers, Metformin treatment (125mg/kg) suppresses pancreatic tumor growth in genetically engineered mice, evidenced by lower tumor volume at the end of study (1 or 3 weeks) [122]. Metformin treatment decreased phosphorylation at both STAT3 and nuclear factor κB [122].

Immunofluorescence imaging showed that Metformin treatment significantly reduced total nuclei, Ki-67 expression (a nuclear proliferation maker), and over a 65% reduction in Ki-67 between control and Metformin treated cells. These findings signify that Metformin treatment (10mM for 48 hours) slowed growth of LL/2 cells, but not entirely abrogated growth. Ki-67 was a particularly important marker to assess as Ki-67 correlates with metastasis and the tumor stage in clinical populations [123]. In light of these positive findings of reduced proliferation, a γ-secretase inhibitor (GSI), small molecule inhibitors preventing the cleave of γ-secretase, was introduced to impede downstream effects of mTOR and in an effort to better assess the potential role of mTOR regulation in proliferation of LL/2 cells. Surprisingly, GSI treatment alone did not

have as stringent of an effect on the LL/2 cells. Staining revealed ~20% reduction in Ki-67 proliferation, which is still auspicious, but nominal compared to Metformin alone. Combining both Metformin treatment with GSI still led to reduced proliferation and ~50% reduction in Ki-67 expression, but again not completely abrogated. This could suggest that growth of NSCLC acts independently of Notch. Since inhibition of γ-secretase, one player in activating Notch, did not completely stop growth of LL/2 cells, it would appear that growth these lung cancers cells is probably not solely regulated via Notch. While inhibiting Notch signaling is effective, it is not the most effective treatment for these cells. Combining Metformin and GSI resulted in a similar effect—significantly reduced growth—rather than a dramatic additive effect.

Metformin is an effective pharmaceutical to reduce cancer cell proliferation, but appears to be more effective when combined with another treatment modality (ie, ionizing radiation, chemotherapeutic, or inhibitor) as noted in other published studies. The reduction in proliferation via Ki-67, suggests Metformin treatment (10mM for 48 hours) does have a positive, anti-proliferative effect, but does not elicit many significant effects when it comes to genes regulating cell cycle progression or proteins involved with cell growth, proliferation, and metabolism. The potential role of Metformin as an anti-cancer intervention still requires further study and may be most beneficial if used as a combination therapy.

4.5 Figures
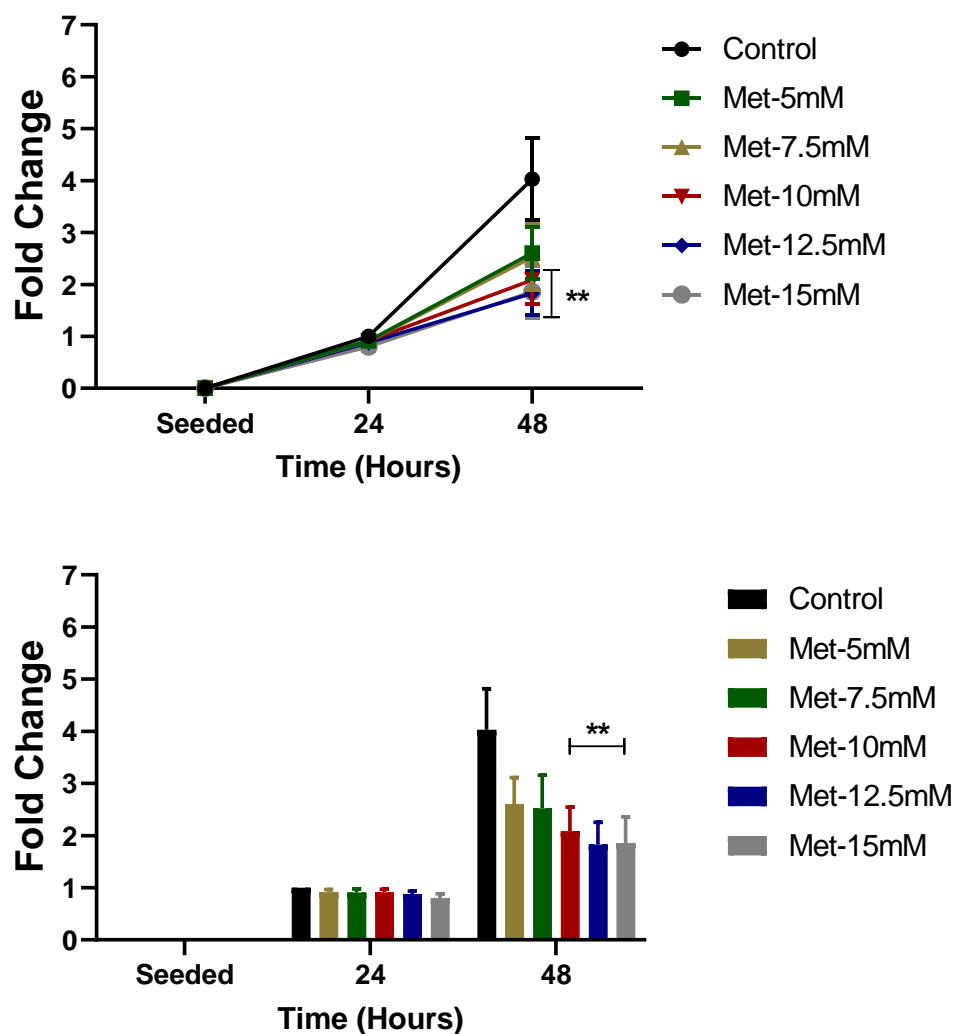
Figure 4.5.1. Proliferation of Lewis Lung Carcinoma Cells following Metformin Treatment over 48 hours. Fold change (relative to control) in proliferating Lewis Lung Carcinoma (LL/2) cells treated with 5mM, 7.5mM, 10mM, 12.5mM or 15mM Metformin for 24 and 48 hours. Data were analyzed using a two-way ANOVA followed by Tukey's multiple comparison test. ** $p<0.01$ vs. Con (n = 5). Data are mean ± SEM.
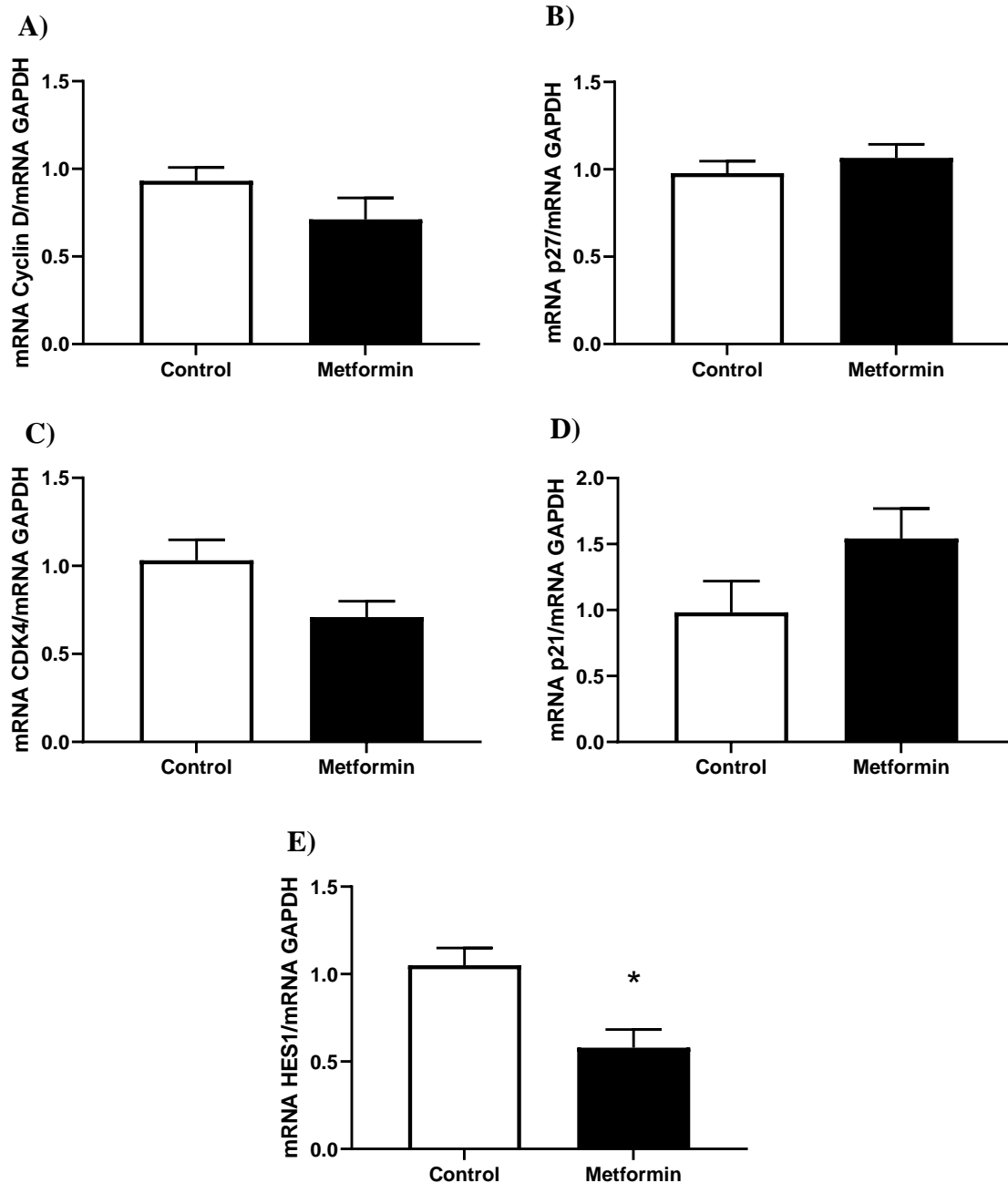
Figure 4.5.2. Gene expression in Lewis Lung Carcinoma Cells treated with 10mM Metformin. A) mRNA Cyclin D/GAPDH; B) mRNA cyclin dependent kinase inhibitor (p27)/GAPDH; C) Cyclin dependent kinase 4 (CDK4)/GAPDH; D) mRNA cyclin dependent kinase inhibitor (p21)/GAPDH; E) mRNA hairy and enhancer of split 1 (Hes1)/GAPDH. mRNA expression in LL/2 cells treated with or without 10mM Metformin. Data were analyzed using an unpaired t-test. *p=0.01 vs Control (n=5). Data are mean ± SEM.
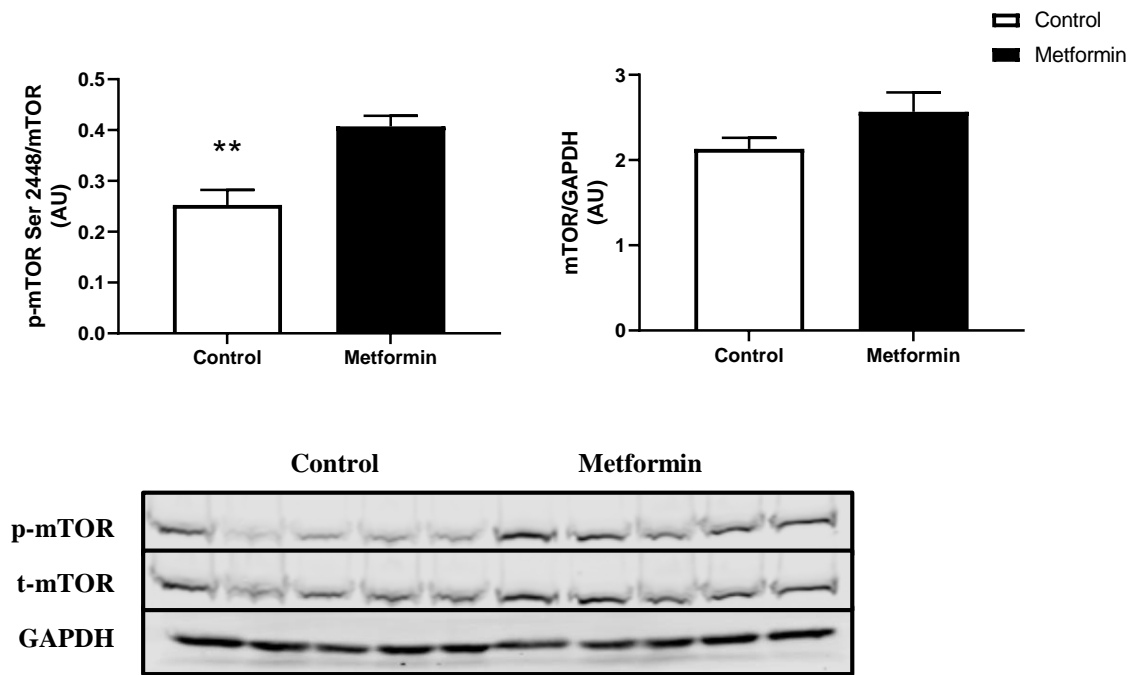
Figure 4.5.3. mTOR expression in Lewis Lung Carcinoma Cells treated with 10mM Metformin. Phospho (p)- mechanistic target of rapamycin (mTOR)/Total mTOR and mTOR/GAPDH expression (Arbitrary Units, AU) in LL/2 cells treated with or without 10mM Metformin. Data were analyzed using an unpaired t-test. **$p<0.01$ vs Control (n=5). Data are mean ± SEM.
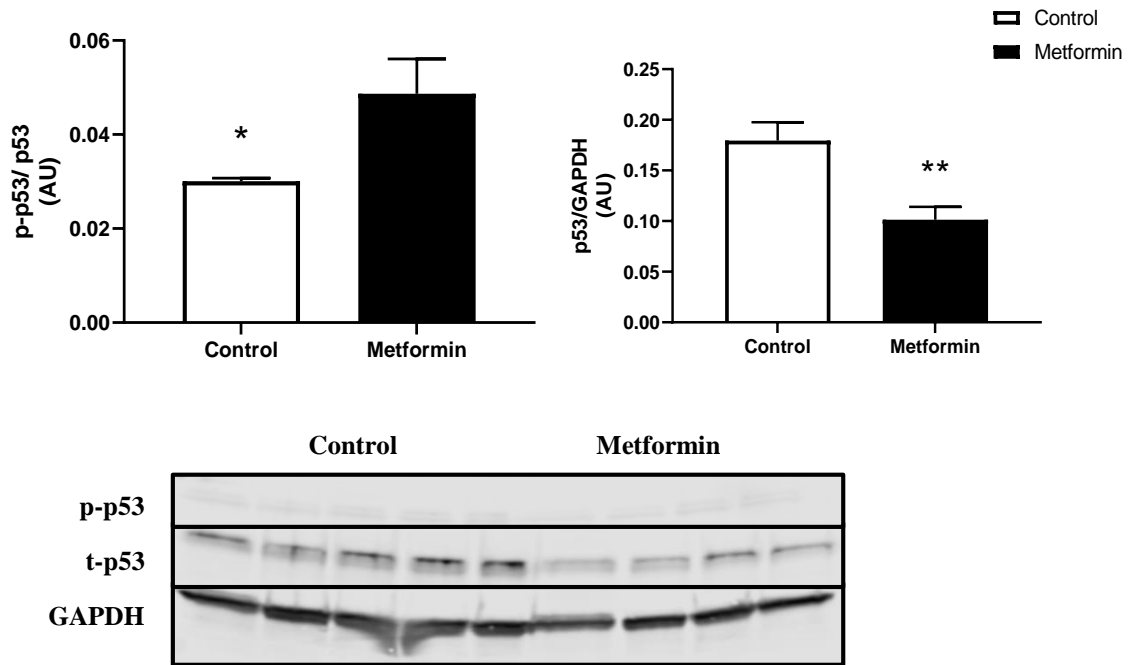
Figure 4.5.4. p53 expression in Lewis Lung Carcinoma Cells treated with 10mM Metformin. Phospho (p)-protein 53(p53)/Total p53 and p53/GAPDH expression (Arbitrary Units, AU) in LL/2 cells treated with or without 10mM Metformin. Data were analyzed using an unpaired t-test. * $p < 0.1$, **$p < 0.01$ vs Control (n=5). Data are mean ± SEM.
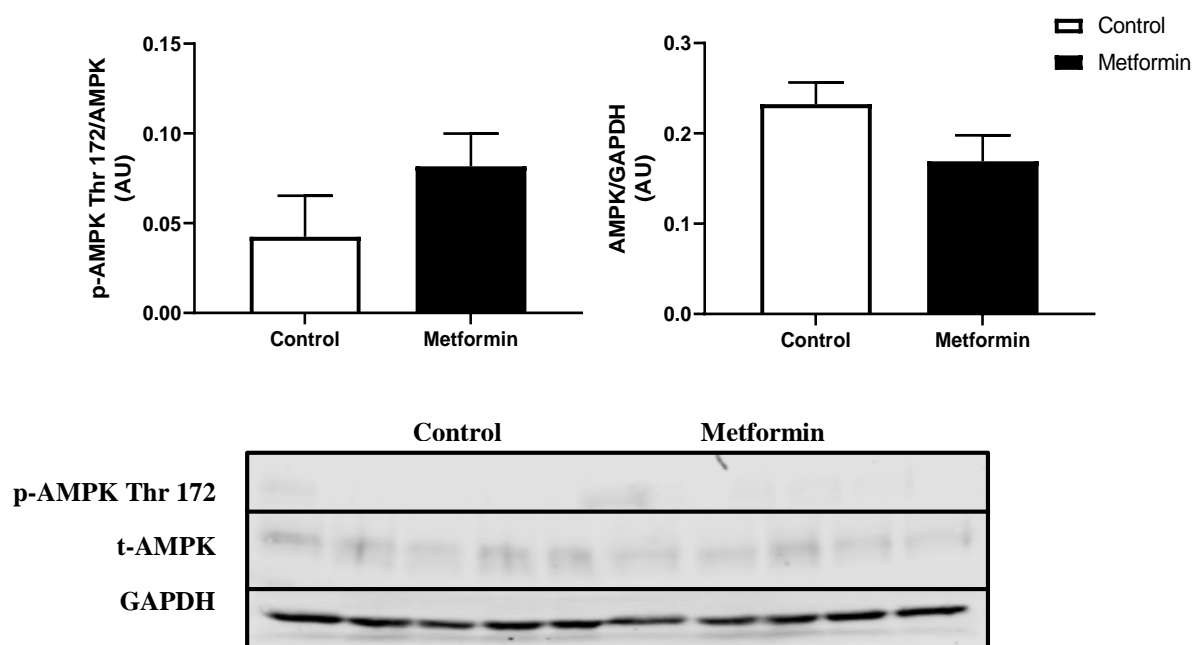
Figure 4.5.5. AMPK expression in Lewis Lung Carcinoma Cells treated with 10mM Metformin. Phospho (p)- adenosine monophosphate-activated protein kinase (AMPK) Thr172/Total AMPK and AMPK/GAPDH expression (Arbitrary Units, AU) in LL/2 cells treated with or without 10mM Metformin. Data were analyzed using an unpaired t-test. Sample size: n=5. Data are mean ± SEM.
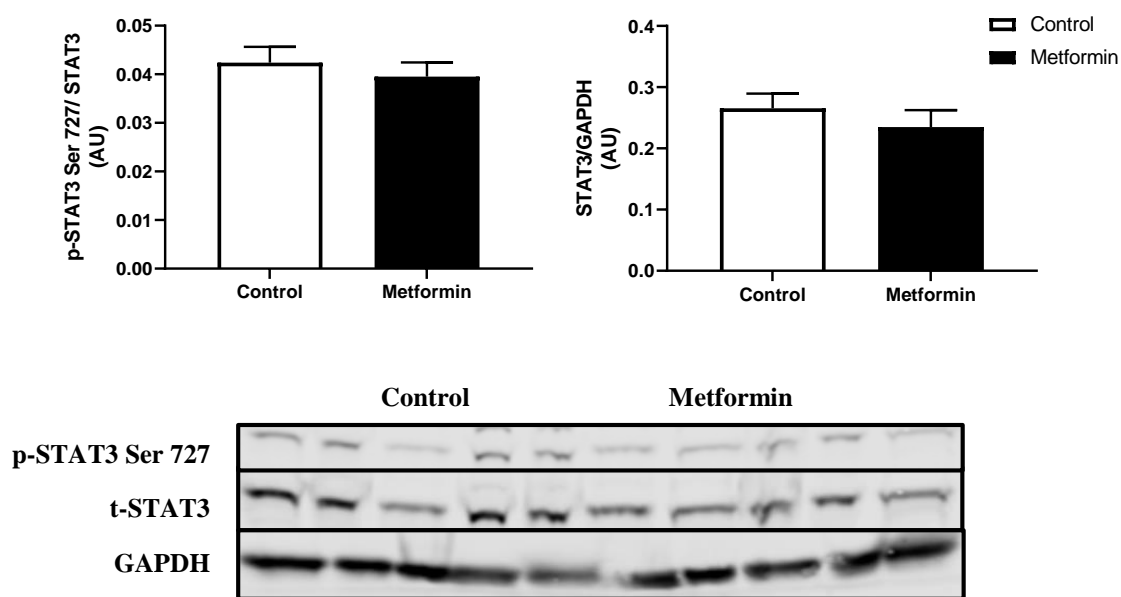
Figure 4.5.6. STAT3 expression in Lewis Lung Carcinoma Cells treated with 10mM Metformin. Phospho (p)- Signal transducer and activator of transcription 3 (STAT3) Ser727/Total STAT3 and STAT3/GAPDH expression (Arbitrary Units, AU) in LL/2 cells treated with or without 10mM Metformin. Data were analyzed using an unpaired t-test. Sample size: n=5. Data are mean ± SEM.
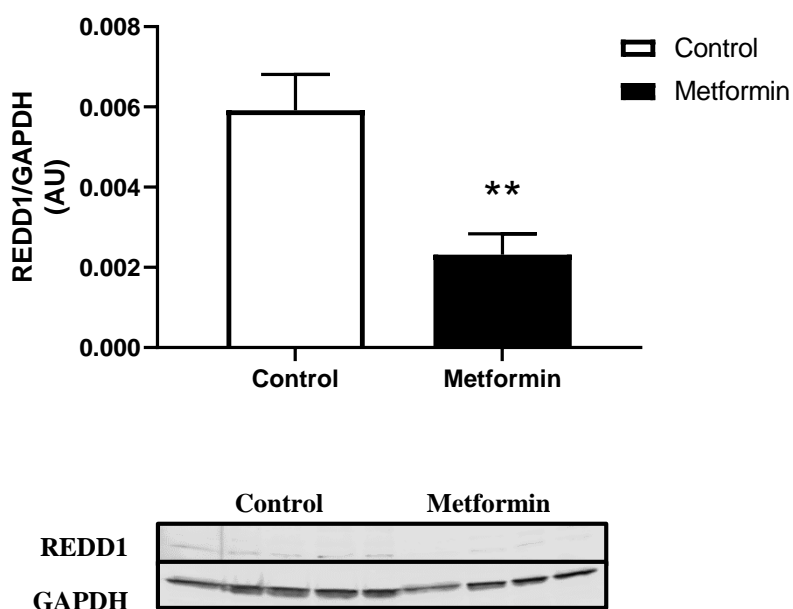
Figure 4.5.7. REDD1 expression in Lewis Lung Carcinoma Cells treated with 10mM Metformin. Regulated in development and DNA damage responses 1 (REDD1)/GAPDH expression (Arbitrary Units, AU) in LL/2 cells treated with or without 10mM Metformin. Data were analyzed using an unpaired t-test. **p<0.01 vs Control (n=5). Data are mean ± SEM.
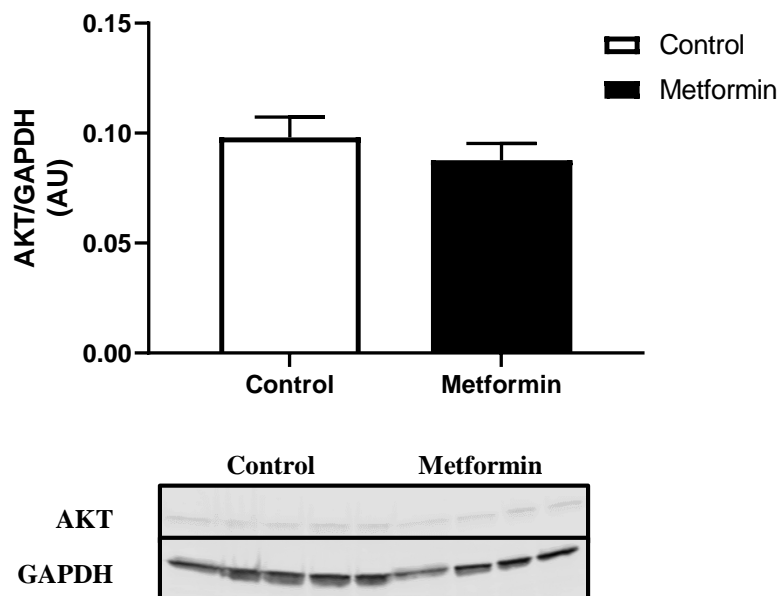
Figure 4.5.8. AKT expression in Lewis Lung Carcinoma Cells treated with 10mM Metformin. Protein kinase B (AKT)/GAPDH expression (Arbitrary Units, AU) in LL/2 cells treated with or without 10mM Metformin. Data were analyzed using an unpaired t-test (p=0.4135). Sample size: n = 5. Data are mean ± SEM.
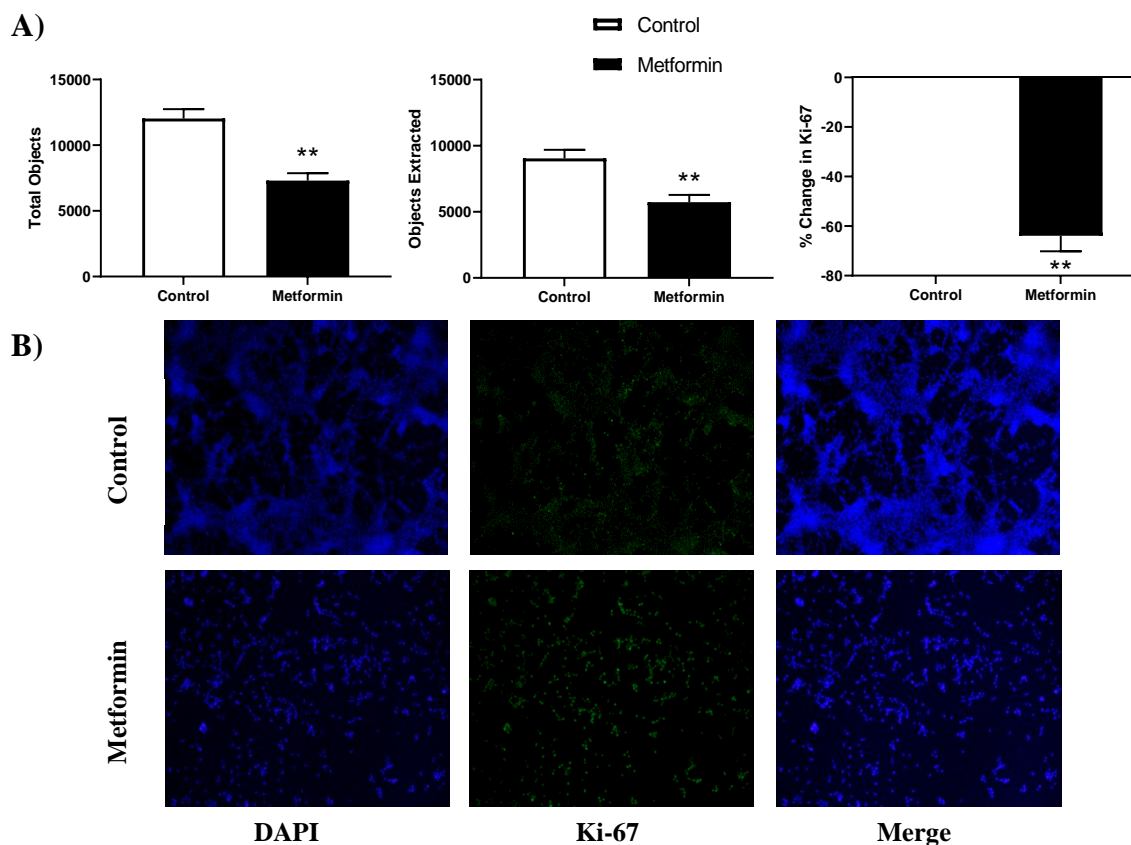
Figure 4.5.9. Ki-67 immunofluorescence in Lewis Lung Carcinoma cells treated with 10mM Metformin. A) Total objects and objects extracted using binary feature extractor via Fiji. Percent change in Ki-67 expression relative to control in 48 hour LL/2 cells treated with or without 10mM Metformin. ** $P < 0.01$ vs. Control (n = 4). Data are mean ± SEM. B) Representative immunofluorescence images of LL/2 cells treated with or without 10mM Metformin using 4',6-diamidino-2-phenylindole (DAPI) and Ki-67 expression visualized via AlexaFluo 488. Representative images were taken at 10x.

A)

B)

DAPI   Ki-67   Merge
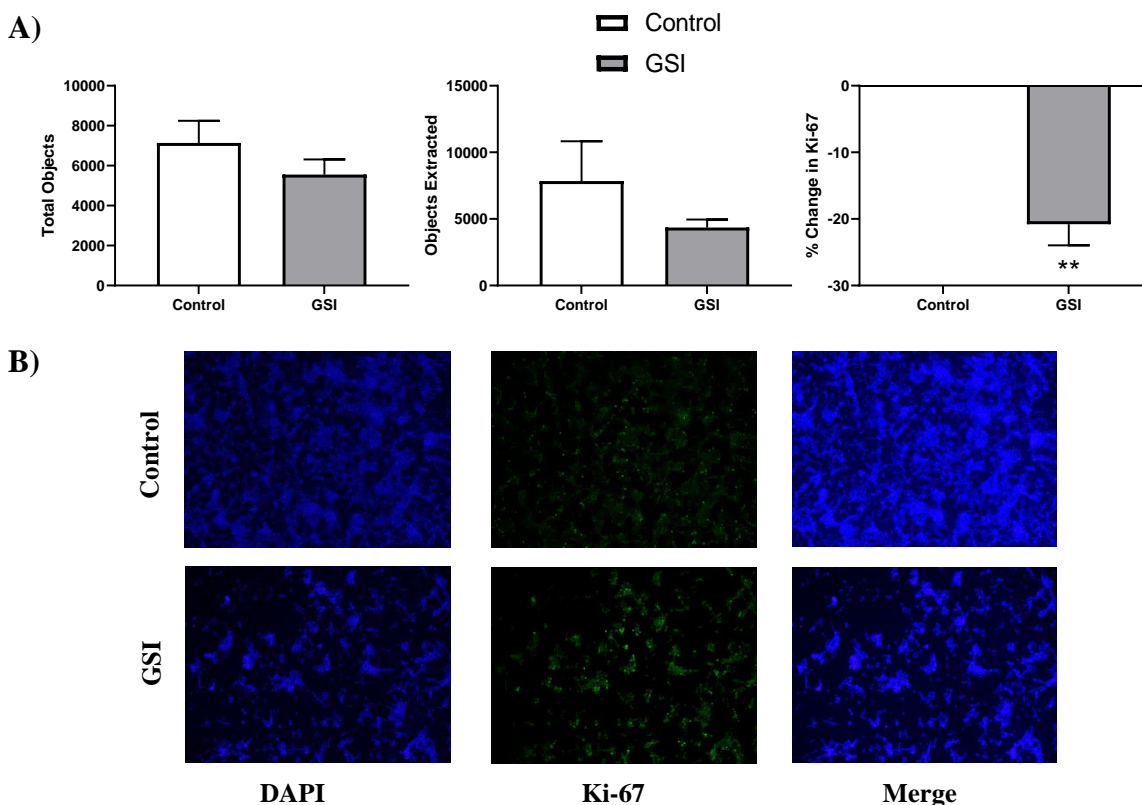
Figure 4.5.10. Ki-67 immunofluorescence in Lewis Lung Carcinoma cells treated with GSI.
A) Total objects and objects extracted using binary feature extractor via Fiji. Percent change in
Ki-67 expression relative to control in 48 hour LL/2 cells treated with or without 4μM Ɣ-
secretase inhibitor (GSI) every 12 hours. ** P < 0.01 vs. Control (n = 5). B) Representative
immunofluorescence images of LL/2 cells treated with or without 10mM Metformin using 4',6-
diamidino-2-phenylindole (DAPI) and Ki-67 expression visualized via AlexaFluo 488.
Representative images were taken at 10x.

A)

B)

DAPI   Ki-67   Merge
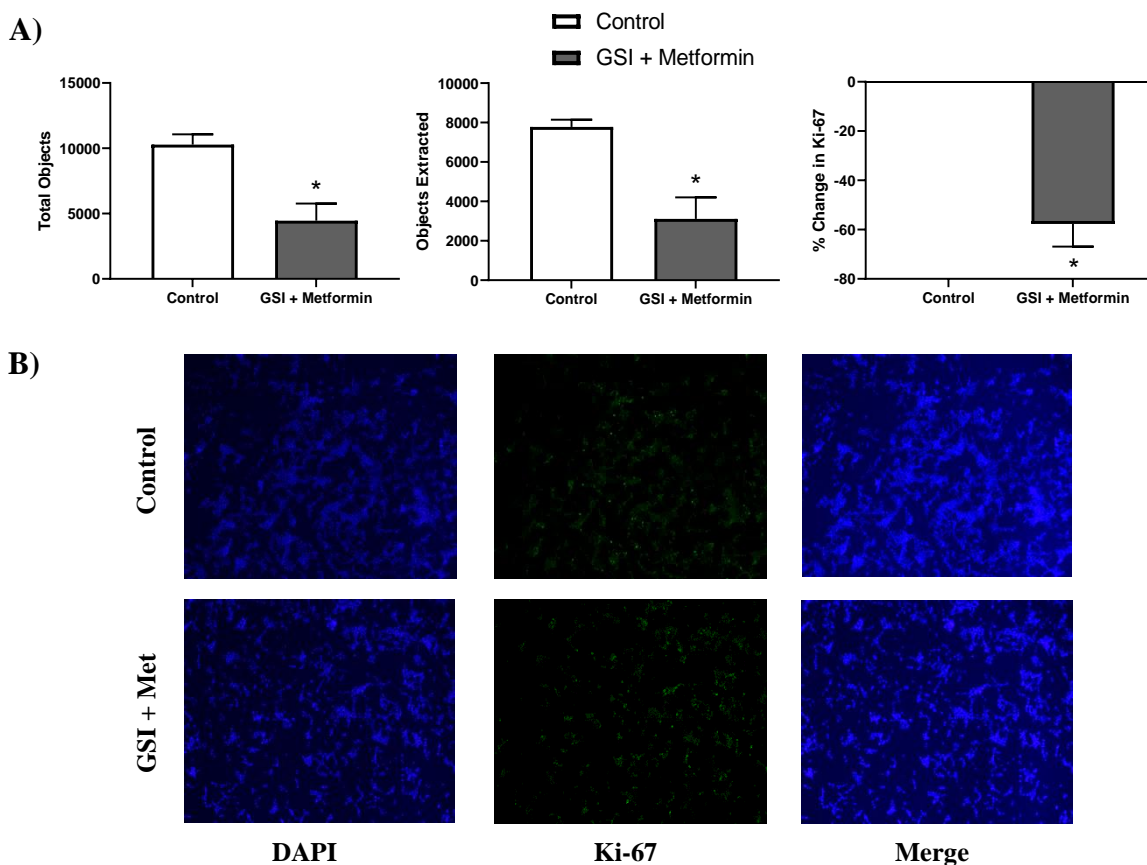
Figure 4.5.11. Ki-67 immunofluorescence in Lewis Lung Carcinoma cells treated with 10mM Metformin. A) Total objects and objects extracted using binary feature extractor via Fiji. Percent change in Ki-67 expression relative to control in 48 hour LL/2 cells treated with or without 10mM Metformin and 4μM Ɣ-secretase inhibitor (GSI) every 12 hours. * P = 0.02 vs. Control (n = 3). B) Representative immunofluorescence images of LL/2 cells treated with or without 10mM Metformin using 4',6-diamidino-2-phenylindole (DAPI) and Ki-67 expression visualized via AlexaFluo 488. Representative images were taken at 10x.

4.6 Tables

Table 4.6.1 Primers used for Gene Expression Analyses.

Primer		Sequence
Cyclin D	Forward	GATGGCGATCGTCCTGTCAT
	Reverse	ACAGGCCGCTACAAGAAACA
CDK4	Forward	ATGGCTGCCACTCGATATGAA
	Reverse	TCCTCCATTAGGAACTCTCACAC
p27	Forward	TCTCTTCGGCCCGGTCAAT
	Reverse	AAATTCCACTTGCGCTGACTC
p21	Forward	TGGTGATGTCCGACCTGTT
	Reverse	CATGAGCGCATCGCAATC
Hes1	Forward	GGTCCTGGAATAGTGCTACCG
	Reverse	CACCGGGGAGGAGGAATTTTT
GAPDH	Forward	ATGTTTGTGATGGGTGTGAA
	Reverse	ATGCCAAAGTTGTCATGGAT

CDK4: Cyclin dependent kinase 4; p27: cyclin dependent kinase inhibitor protein 27; p21: cyclin dependent kinase inhibitor protein 21; Hes1: Hairy and enhancer split protein; GAPDH: Glyceraldehyde 3-Phosphate Dehydrogenase

Table 4.6.2 Primary Antibodies used for Western Blot Analyses.

Antibody	Catalog #, Company	Dilution
Phospho AMPK Thr 172	(#4188; CS)	1: 500
AMPK	(#2532; CS)	1: 500
P-mTOR Ser2448	(#5536; CS)	1: 500
Total mTOR	(#4517; CS)	1: 500
P-p53 Ser392	(#9281, CS)	1: 500
Total p53	(#32532, CS)	1: 500
P-STAT3 Ser727	(#9134; CS)	1: 500
Total STAT3	(#4904, CS)	1: 500
Phospho AKT Thr308	(#9275; CS)	1: 500
Phospho AKT Ser473	(#9271; CS)	1: 500
Total AKT	(#2920; CS)	1: 500
REDD1	(#PIPA520495; FS)	1:1000
GAPDH	(#MAB374; CS)	1:5000

AMPK: 5' Adenosine Monophosphate-Activated Protein Kinase; mTOR: mechanistic target of rampamycin; Ser: Serine; p53: Protein 53; STAT3: Signal transducer and activator transcription 3; AKT: Protein Kinase B (PKB); Thr: Threonine; REDD1: Regulated in development and DNA damage responses; GAPDH: Glyceraldehyde 3-phosphate dehydrogenase; CS: Cell signaling; FS: FisherScientific

Table 4.6.3 Primary and Secondary Antibodies used for Immunofluorescence.

Antibody	**Catalog #, Company**	**Dilution**
Ki-67	(#9129, CS)	1:400
GT-Anti Rab IgG 488	(#A11008,TF)	1:1000

GT: goat; Rab: Rabbit; IgG: immunoglobulin G; CS: Cell signaling; TF: ThermoFisher

CHAPTER 5: DISSERTATION DISCUSSION

Lung cancer is responsible for 1.6 million deaths worldwide [60]. In the United States, the yearly diagnoses are expected to reach 225,000 in 2030 [3]. While cigarette smoke is one of the largest contributors to lung cancer diagnoses, a combination of lifestyle, genetic, and environmental components increase risk of developing lung cancer [4]. Non-Small Cell Lung Carcinoma (NSCLC) remains more prominent—making up 80-85% of all lung cancer diagnoses [4]. Even with phenomenal strides in cancer therapies over the years, the relative survival rate for lung cancer patients remains at a modest 20% (SEER, National Cancer Institute). The prevalence of NSCLC diagnoses indicates there is still a great need to find measures to diminish lung cancer risk, decrease tumor progression, reduce the burden of diagnoses, and target improved therapies for these patients.

Literature widely shows the potential efficacy of repositioning Metformin as a therapeutic for targeting cancers, in particular breast, prostate, colon and thyroid cancer [32-36]. However, the effectiveness and potential role of this pharmaceutical on NSCLC growth is not fully characterized. Understanding the effect of Metformin on both NSLCLC growth and overall skeletal muscle health could lead to the potential use Metformin more efficiently and through better-targeted means for NSCLC treatment. This project assessed how well Metformin combated tumorigenesis in immunocompetent mice subject to an orthotopic model of lung cancer and how skeletal muscle health was affected during tumor development. We expected to see reduced tumor growth and longevity in Metformin treated animals concomitant with less atrophy in skeletal muscle. We also anticipated to see a staunch reduction in NSCLC proliferation *in vitro* associated with gene and protein expression reflecting these anti-neoplastic effects.

This dissertation led to the following findings: 1) Metformin treatment (250mg/kg) given intraperitoneally twice weekly is not sufficient to reduce Lewis Lung Carcinoma tumor growth or burden in an immunocompetent orthotopic mouse model of LL/2 (Chapter 2). 2) Skeletal muscle did not exhibit detectable changes in muscle mass and metabolism during this short (< 6 weeks) orthotopic model of LL/2 (Chapter 3). 3) Metformin treatment ($\geq$10mM over 48 hours) is sufficient to reduce tumor cell growth *in vitro*; however, not all gene and protein expression markers representative of cell growth, cell cycle regulation, and metabolism mirrored the curtailed NSCLC proliferation. (Chapter 4).

Our findings *in vivo* do conflict with much of the literature pointing to the advantageous effects of Metformin usage within the realm of cancer treatments. While Metformin is widely used in clinical studies to combat cancer, the efficacy of Metformin in this immunocompetent mouse model proved to be ineffective in directly slowing tumor growth. Although Metformin treated mice did consume a higher caloric intake over the course of the study and maintain better body mass overall, the impact of Metformin did not result in significant reductions of tumor growth. In particular, cell cycle regulators did trend in some cases toward slowed growth, but this shifting was not significant enough to extend the longevity nor reduce the tumor burden. It would appear that Metformin did not directly affect the tumor *in vivo* as we hoped.

These surprising findings are likely rooted in both the route of delivery and timing of Metformin dosing. When Metformin is given in clinical populations to combat high blood glucose levels in Type 2 Diabetics, dosing is typically seen twice a day, resulting in much higher bioavailability. Importantly, the majority of Metformin is absorbed within the small intestine [124], resulting in a higher absorption within the abdominal region rather than the thoracic region, which was the site of the tumor in this Lewis Lung Cancer model. Metformin's efficacy

is largely dependent on how readily Metformin can be transported across cell membranes through organic cation ion transporters [41]. Because metformin is a hydrophilic base it does not readily under undergo passive diffusion across cell membranes [125]. Following administration, peak concentrations of Metformin occur within ~3 hours and absorption ceases in 6-10 hours, with ~95% excreted via urine within 8 hours [126]. In subjects without any issues in renal function, the clearance rate of Metformin is 507 ± 129 mL/min, suggesting that Metformin is readily filtered and eliminated [126]. Since the half-life of Metformin ranges from 1.5-6.5 hours, there is no doubt that Metformin treatments in this model of NSCLC were insufficient to provide sustained bioavailability [69]. Furthermore, mice treated with Metformin through drinking water, rather than IP injections, lead to an average of 32µM (range of 9.1-55.7µM) in blood plasma levels, allowing more consistent drug delivery to the tumor site [71].

In contrast to our findings, a xenograft model of ovarian cancer in immunocompromised mice receiving Metformin (250mg/kg/day) had fewer ovarian tumors over 4 weeks [112]. In contrast to the present study, Lengyel et al. administered Metformin more frequently and at a dose 6-fold higher than the present study, leading to an increase in the bioavailabity of Metformin to all animals with ovarian cancer [112]. Furthermore, the lack of a thymus does change the microenvironment surrounding the tumor and systemically, as macrophage infiltration and other immune responses would be absent. In light of nearly 100% clearance of Metformin through renal circulation, this suggests that Metformin really had no traction to combat tumor growth in the present LL/2 model, especially since the pharmaceutical was cleared at a high rate (nearly 95% clearance within 8 hours [126]) and given twice a week instead of daily. To overcome this challenge, refinement for drug delivery could be adjusted to better determine the direct effect Metformin may have on tumor growth *in vivo*.

Nanoparticles possess many unique characteristics, making them excellent vehicles for drug delivery and creating a more targeted approach of medication delivery to tumors [74]. This could create the potential for increased bioavailability of the drug within the tumor microenvironment and better regulate pharmacokinetic effects [75]. For many years, nanoparticle gene therapy *in vitro* and *in vivo* proves to be an effective route for both cellular transfection and targeting lung cancer tumors, systemically and locally [73]. Specifically in NSCLC lines, nanoparticle carriers encapsulated biomolecules and successfully reached target tissues, resulting in either silencing or knockdown of genes to attenuate tumor cell growth [76, 77]. However, nanoparticle delivery does provide some challenges as these platforms are implemented into the clinical population. In particular, the stability of the nanoparticle upon delivery, penetrability of larger biological membranes, the potential cytotoxicity from the nanoparticles, and the heterogeneity of nanoparticles required for specific drug delivery.

The orthotopic tumor injection utilized in this study did not allow for direct development of rapid cachexia, as seen in other cachexia animal models when cancer is directly injected into the flank of animals [90, 99]. Since the timeline in this study was short (<6 weeks), it is probable that potential changes in gastrocnemius skeletal muscle mass were not induced, especially since irradiation or strong therapeutics known to have deleterious effects on skeletal muscle health were not utilized as co-treatments in this study [9]. It would be advantageous to pursue co-treatment modalities, with Metformin as a potentially supportive drug rather than a monotherapy to mitigate cancer progression [127]. This could still allow stronger drugs to target tumor progression, but use Metformin to combat the secondary effects occurring in skeletal muscle.

Based off the present study, Metformin treatment (10mM for 48 hours) alone is not sufficient to completely abrogate LL/2 cell growth *in vitro*. The reduction in proliferation via Ki-

67, suggests Metformin treatment (10mM for 48 hours) does have a positive, anti-proliferative effect, but does not elicit many significant effects when it comes to genes regulating cell cycle progression or proteins involved with cell growth, proliferation, and metabolism. Importantly, since GSI did not fully blunt NSCLC proliferation, it is highly probably that NSCLC growth is not solely regulated via Notch signaling. Metformin (10mM for 48 hours) is an effective pharmaceutical to reduce cancer cell proliferation when directly added to LL/2 cells *in vitro*, but the potential role of Metformin as an anti-cancer intervention for NSCLC, with the potential for more successful translatability, still requires further study and may be most beneficial if Metformin is not used as a monotherapy.

Notably these findings led us to conclude that Metformin treatment, while exhibiting many anti-neoplastic characteristics for many other cancers, may not be the best monotherapy for NSCLC tumor growth *in vitro* or *in vivo*. While these findings do not lead us directly to more targeted care for patients, these steps are important to take as research continues to evolve. Many signaling pathways intersect and a multitude of factors compound, making development of therapies and treatment of cancer an on-going challenge for scientists and health care professionals. Future studies should be conducted to further investigate Metformin as a co-therapy and approached with more targeted drug delivery tactics. If combination therapies with Metformin can elicit protective effects, namely preservation of satellite cells and upregulation of genes protecting against catabolic activity, in skeletal muscle during chemotherapy or radiation, it could have the potential to improve patient outcomes throughout cancer treatment. Ultimately, opening the potential for contributing more clinically meaningful improvements and measures to improve their quality of life even in remission.

REFERENCES

1. Ikhlas, S. and M. Ahmad, *Metformin: Insights into its anticancer potential with special reference to AMPK dependent and independent pathways.* Life Sci, 2017. **185**: p. 53-62.
2. Society., A.C., *Cancer Facts and Figures 2019.* 2019: Atlanta.
3. Rahib, L., et al., *Projecting cancer incidence and deaths to 2030: the unexpected burden of thyroid, liver, and pancreas cancers in the United States.* Cancer Res, 2014. **74**(11): p. 2913-21.
4. Molina, J.R., et al., *Non-small cell lung cancer: epidemiology, risk factors, treatment, and survivorship.* Mayo Clin Proc, 2008. **83**(5): p. 584-94.
5. Eymin, B. and S. Gazzeri, *Role of cell cycle regulators in lung carcinogenesis.* Cell Adh Migr, 2010. **4**(1): p. 114-23.
6. Vesely, M.D., et al., *Natural innate and adaptive immunity to cancer.* Annu Rev Immunol, 2011. **29**: p. 235-71.
7. Hirsch, F.R., et al., *Lung cancer: current therapies and new targeted treatments.* The Lancet, 2017. **389**(10066): p. 299-311.
8. Zierath, J.R. and H. Wallberg-Henriksson, *From receptor to effector: insulin signal transduction in skeletal muscle from type II diabetic patients.* Ann N Y Acad Sci, 2002. **967**: p. 120-34.
9. Burckart, K., et al., *Pathogenesis of muscle wasting in cancer cachexia: targeted anabolic and anticatabolic therapies.* Curr Opin Clin Nutr Metab Care, 2010. **13**(4): p. 410-6.
10. Baracos, V.E., et al., *Cancer-associated cachexia.* Nature Reviews Disease Primers, 2018. **4**: p. 17105.
11. Evans, W.J., *Skeletal muscle loss: cachexia, sarcopenia, and inactivity.* Am J Clin Nutr, 2010. **91**(4): p. 1123S-1127S.
12. Sorensen, J., *Lung Cancer Cachexia: Can Molecular Understanding Guide Clinical Management?* Integr Cancer Ther, 2018. **17**(3): p. 1000-1008.
13. Aniort, J., et al., *Muscle wasting in patients with end-stage renal disease or early-stage lung cancer: common mechanisms at work.* J Cachexia Sarcopenia Muscle, 2019. **10**(2): p. 323-337.
14. Rudrappa, S.S., et al., *Human Skeletal Muscle Disuse Atrophy: Effects on Muscle Protein Synthesis, Breakdown, and Insulin Resistance-A Qualitative Review.* Front Physiol, 2016. **7**: p. 361.
15. Tisdale, M.J., *Cancer cachexia.* Curr Opin Gastroenterol, 2010. **26**(2): p. 146-51.
16. Tisdale, M.J., *Protein Loss in Cancer Cachexia.* Science, 2000. **289**(5488): p. 2293-2294.
17. de Castro, G.S., et al., *Human Cachexia Induces Changes in Mitochondria, Autophagy and Apoptosis in the Skeletal Muscle.* Cancers (Basel), 2019. **11**(9).
18. Hirsch, F.R., et al., *New and emerging targeted treatments in advanced non-small-cell lung cancer.* The Lancet, 2016. **388**(10048): p. 1012-1024.
19. Williams, C.T., *Food and Drug Administration Drug Approval Process: A History and Overview.* Nurs Clin North Am, 2016. **51**(1): p. 1-11.
20. Sleire, L., et al., *Drug repurposing in cancer.* Pharmacol Res, 2017. **124**: p. 74-91.
21. Morales, D.R. and A.D. Morris, *Metformin in cancer treatment and prevention.* Annu Rev Med, 2015. **66**: p. 17-29.
22. Tsai, M.J., et al., *Metformin decreases lung cancer risk in diabetic patients in a dose-dependent manner.* Lung Cancer, 2014. **86**(2): p. 137-43.
23. Lin, J., et al., *Metformin use and survival after non-small cell lung cancer: A cohort study in the US Military health system.* Int J Cancer, 2017. **141**(2): p. 254-263.
24. Rena, G., D.G. Hardie, and E.R. Pearson, *The mechanisms of action of metformin.* Diabetologia, 2017. **60**(9): p. 1577-1585.

25.   Zhang, X., et al., *Unraveling the Regulation of Hepatic Gluconeogenesis.* Front Endocrinol (Lausanne), 2018. **9**: p. 802.

26.   Sousa, J.S., E. D'Imprima, and J. Vonck, *Mitochondrial Respiratory Chain Complexes*, in *Membrane Protein Complexes: Structure and Function*, J.R. Harris and E.J. Boekema, Editors. 2018, Springer Singapore: Singapore. p. 167-227.

27.   Fontaine, E., *Metformin-Induced Mitochondrial Complex I Inhibition: Facts, Uncertainties, and Consequences.* Front Endocrinol (Lausanne), 2018. **9**: p. 753.

28.   Pavlidou, T., et al., *Metformin Delays Satellite Cell Activation and Maintains Quiescence.* Stem Cells Int, 2019. **2019**: p. 5980465.

29.   Yin, H., F. Price, and M.A. Rudnicki, *Satellite cells and the muscle stem cell niche.* Physiol Rev, 2013. **93**(1): p. 23-67.

30.   Suwa, M., et al., *Metformin increases the PGC-1alpha protein and oxidative enzyme activities possibly via AMPK phosphorylation in skeletal muscle in vivo.* J Appl Physiol (1985), 2006. **101**(6): p. 1685-92.

31.   Sandri, M., et al., *PGC-1alpha protects skeletal muscle from atrophy by suppressing FoxO3 action and atrophy-specific gene transcription.* Proc Natl Acad Sci U S A, 2006. **103**(44): p. 16260-5.

32.   Sarmento-Cabral, A., et al., *Metformin Reduces Prostate Tumor Growth, in a Diet-Dependent Manner, by Modulating Multiple Signaling Pathways.* Mol Cancer Res, 2017. **15**(7): p. 862-874.

33.   Checkley, L.A., et al., *Metformin inhibits skin tumor promotion in overweight and obese mice.* Cancer Prev Res (Phila), 2014. **7**(1): p. 54-64.

34.   Algire, C., et al., *Metformin blocks the stimulative effect of a high-energy diet on colon carcinoma growth in vivo and is associated with reduced expression of fatty acid synthase.* Endocr Relat Cancer, 2010. **17**(2): p. 351-60.

35.   Park, J. and e. al, *Metformin blocks progression of obesity-activated thyroid cancer in a mouse model.* Oncotarget, 2016. **7**(23): p. 34832-44.

36.   Queiroz, E.A., et al., *Metformin induces apoptosis and cell cycle arrest mediated by oxidative stress, AMPK and FOXO3a in MCF-7 breast cancer cells.* PLoS One, 2014. **9**(5): p. e98207.

37.   Lei, Y., et al., *Metformin targets multiple signaling pathways in cancer.* Chin J Cancer, 2017. **36**(1): p. 17.

38.   Tan, X.L., et al., *Metformin suppresses pancreatic tumor growth with inhibition of NFkappaB/STAT3 inflammatory signaling.* Pancreas, 2015. **44**(4): p. 636-47.

39.   Memmott, R.M., et al., *Metformin prevents tobacco carcinogen--induced lung tumorigenesis.* Cancer Prev Res (Phila), 2010. **3**(9): p. 1066-76.

40.   Saisho, Y., *Metformin and Inflammation: Its Potential Beyond Glucose-lowering Effect.* Endocr Metab Immune Disord Drug Targets, 2015. **15**(3): p. 196-205.

41.   Yang, J., et al., *Renal tumours in a Tsc1+/- mouse model show epigenetic suppression of organic cation transporters Slc22a1, Slc22a2 and Slc22a3, and do not respond to metformin.* Eur J Cancer, 2013. **49**(6): p. 1479-90.

42.   Shu, Y., et al., *Effect of genetic variation in the organic cation transporter 1 (OCT1) on metformin action.* J Clin Invest, 2007. **117**(5): p. 1422-31.

43.   Willows, R., et al., *Phosphorylation of AMPK by upstream kinases is required for activity in mammalian cells.* Biochem J, 2017. **474**(17): p. 3059-3073.

44.   Inoki, K., T. Zhu, and K.L. Guan, *TSC2 mediates cellular energy response to control cell growth and survival.* Cell, 2003. **115**(5): p. 577-90.

45.   Lee, C.W., et al., *AMPK promotes p53 acetylation via phosphorylation and inactivation of SIRT1 in liver cancer cells.* Cancer Res, 2012. **72**(17): p. 4394-404.

46.   Irie, H., et al., *Metformin: A candidate for the treatment of gynecological tumors based on drug repositioning.* Oncol Lett, 2016. **11**(2): p. 1287-1293.

47.   Ben Sahra, I., et al., *Metformin, independent of AMPK, induces mTOR inhibition and cell-cycle arrest through REDD1.* Cancer Res, 2011. **71**(13): p. 4366-72.

48.   Karnevi, E., et al., *Metformin-mediated growth inhibition involves suppression of the IGF-I receptor signalling pathway in human pancreatic cancer cells.* BMC Cancer, 2013. **13**(1): p. 235.

49.   Cai, S.L., et al., *Activity of TSC2 is inhibited by AKT-mediated phosphorylation and membrane partitioning.* J Cell Biol, 2006. **173**(2): p. 279-89.

50.   Luo, Z., et al., *Metformin promotes survivin degradation through AMPK/PKA/GSK-3beta-axis in non-small cell lung cancer.* J Cell Biochem, 2019.

51.   Brown, J.L., et al., *Protein imbalance in the development of skeletal muscle wasting in tumour-bearing mice.* J Cachexia Sarcopenia Muscle, 2018. **9**(5): p. 987-1002.

52.   Constantinou, C., et al., *Nuclear magnetic resonance in conjunction with functional genomics suggests mitochondrial dysfunction in a murine model of cancer cachexia.* Int J Mol Med, 2011. **27**(1): p. 15-24.

53.   Hemmings, B.A. and D.F. Restuccia, *PI3K-PKB/Akt pathway.* Cold Spring Harb Perspect Biol, 2012. **4**(9): p. a011189.

54.   Oliveira, A.G. and M.C. Gomes-Marcondes, *Metformin treatment modulates the tumour-induced wasting effects in muscle protein metabolism minimising the cachexia in tumour-bearing rats.* BMC Cancer, 2016. **16**: p. 418.

55.   Mordant, P., et al., *Bioluminescent orthotopic mouse models of human localized non-small cell lung cancer: feasibility and identification of circulating tumour cells.* PLoS One, 2011. **6**(10): p. e26073.

56.   Kellar, A., C. Egan, and D. Morris, *Preclinical Murine Models for Lung Cancer: Clinical Trial Applications.* Biomed Res Int, 2015. **2015**: p. 621324.

57.   Ning, T., et al., *Gene therapy with the angiogenesis inhibitor endostatin in an orthotopic lung cancer murine model.* Hum Gene Ther, 2009. **20**(2): p. 103-11.

58.   Murakami, K., et al., *4-[3,5-Bis(trimethylsilyl)benzamido] benzoic acid (TAC-101) inhibits the intrahepatic spread of hepatocellular carcinoma and prolongs the life-span of tumor-bearing animals.* Clin Exp Metastasis, 1998. **16**(7): p. 633-43.

59.   Poczobutt, J.M., et al., *Eicosanoid profiling in an orthotopic model of lung cancer progression by mass spectrometry demonstrates selective production of leukotrienes by inflammatory cells of the microenvironment.* PLoS One, 2013. **8**(11): p. e79633.

60.   Society, A.C., *Cancer Facts & Figures 2018.* 2018, American Cancer Society: Atlanta, Ga. p. 1-76.

61.   Zakikhani, M., et al., *Metformin is an AMP kinase-dependent growth inhibitor for breast cancer cells.* Cancer Res, 2006. **66**(21): p. 10269-73.

62.   Park, J.W., et al., *Sex-dependent difference in the effect of metformin on colorectal cancer-specific mortality of diabetic colorectal cancer patients.* World J Gastroenterol, 2017. **23**(28): p. 5196-5205.

63.   Zhu, N., et al., *Metformin and lung cancer risk of patients with type 2 diabetes mellitus: A meta-analysis.* Biomed Rep, 2015. **3**(2): p. 235-241.

64.   Tseng, C.H., *Metformin and lung cancer risk in patients with type 2 diabetes mellitus.* Oncotarget, 2017. **8**(25): p. 41132-41142.

65.   Hung, M.S., et al., *Metformin Prolongs Survival in Type 2 Diabetes Lung Cancer Patients With EGFR-TKIs.* Integr Cancer Ther, 2019. **18**: p. 1534735419869491.

66.   Ogawa, F., et al., *Aspirin reduces lung cancer metastasis to regional lymph nodes.* Biomed Pharmacother, 2014. **68**(1): p. 79-86.

67.   Lengyel, E., et al., *Metformin inhibits ovarian cancer growth and increases sensitivity to paclitaxel in mouse models.* Am J Obstet Gynecol, 2015. **212**(4): p. 479.e1-479.e10.

68.   Latteyer, S., et al., *Thyroxine promotes lung cancer growth in an orthotopic mouse model.* Endocr Relat Cancer, 2019. **26**(6): p. 565-574.

69.   Pernicova, I. and M. Korbonits, *Metformin--mode of action and clinical implications for diabetes and cancer.* Nat Rev Endocrinol, 2014. **10**(3): p. 143-56.

70.   Bailey, C.J. and R.C. Turner, *Metformin.* N Engl J Med, 1996. **334**(9): p. 574-9.

71.	Dowling, R.J., et al., *Metformin Pharmacokinetics in Mouse Tumors: Implications for Human Therapy.* Cell Metab, 2016. **23**(4): p. 567-8.

72.	Heinig, K. and F. Bucheli, *Fast liquid chromatographic-tandem mass spectrometric (LC-MS-MS) determination of metformin in plasma samples.* J Pharm Biomed Anal, 2004. **34**(5): p. 1005-11.

73.	Lee, H.Y., K.A. Mohammed, and N. Nasreen, *Nanoparticle-based targeted gene therapy for lung cancer.* Am J Cancer Res, 2016. **6**(5): p. 1118-34.

74.	Duncan, R. and R. Gaspar, *Nanomedicine(s) under the microscope.* Mol Pharm, 2011. **8**(6): p. 2101-41.

75.	Chaudhary, S., et al., *Strategic targeting of non-small-cell lung cancer utilizing genetic material-based delivery platforms of nanotechnology.* J Biochem Mol Toxicol, 2021: p. e22784.

76.	Bai, J., et al., *Engineered targeting tLyp-1 exosomes as gene therapy vectors for efficient delivery of siRNA into lung cancer cells.* Asian J Pharm Sci, 2020. **15**(4): p. 461-471.

77.	Mehta, A., et al., *Targeting KRAS Mutant Lung Cancer Cells with siRNA-Loaded Bovine Serum Albumin Nanoparticles.* Pharm Res, 2019. **36**(9): p. 133.

78.	Knüpfer, H. and R. Preiss, *Serum interleukin-6 levels in colorectal cancer patients—a summary of published results.* International Journal of Colorectal Disease, 2010. **25**(2): p. 135-140.

79.	Zhao, Z., et al., *Metformin Inhibits the IL-6-Induced Epithelial-Mesenchymal Transition and Lung Adenocarcinoma Growth and Metastasis.* PLOS ONE, 2014. **9**(4): p. e95884.

80.	Ding, L., et al., *Metformin prevents cancer metastasis by inhibiting M2-like polarization of tumor associated macrophages.* Oncotarget, 2015. **6**(34): p. 36441-55.

81.	Wang, S., et al., *Low-Dose Metformin Reprograms the Tumor Immune Microenvironment in Human Esophageal Cancer: Results of a Phase II Clinical Trial.* Clin Cancer Res, 2020. **26**(18): p. 4921-4932.

82.	Liu, Q., et al., *Metformin Inhibits Prostate Cancer Progression by Targeting Tumor-Associated Inflammatory Infiltration.* Clin Cancer Res, 2018. **24**(22): p. 5622-5634.

83.	Aoyagi, T., et al., *Cancer cachexia, mechanism and treatment.* World J Gastrointest Oncol, 2015. **7**(4): p. 17-29.

84.	Schmidt, S.F., et al., *Cancer Cachexia: More Than Skeletal Muscle Wasting.* Trends Cancer, 2018. **4**(12): p. 849-860.

85.	Currow, D.C., et al., *Efficacy of Anamorelin, a Novel Non-Peptide Ghrelin Analogue, in Patients with Advanced Non-Small Cell Lung Cancer (NSCLC) and Cachexia-Review and Expert Opinion.* Int J Mol Sci, 2018. **19**(11).

86.	LeBlanc, T.W., et al., *Correlation between the international consensus definition of the Cancer Anorexia-Cachexia Syndrome (CACS) and patient-centered outcomes in advanced non-small cell lung cancer.* J Pain Symptom Manage, 2015. **49**(4): p. 680-9.

87.	Fearon, K.C., A.C. Voss, and D.S. Hustead, *Definition of cancer cachexia: effect of weight loss, reduced food intake, and systemic inflammation on functional status and prognosis.* Am J Clin Nutr, 2006. **83**(6): p. 1345-50.

88.	Brown, J.L., et al., *Mitochondrial degeneration precedes the development of muscle atrophy in progression of cancer cachexia in tumour-bearing mice.* J Cachexia Sarcopenia Muscle, 2017. **8**(6): p. 926-938.

89.	Fink, L.N., et al., *Pro-inflammatory macrophages increase in skeletal muscle of high fat-fed mice and correlate with metabolic risk markers in humans.* Obesity (Silver Spring), 2014. **22**(3): p. 747-57.

90.	Ham, D.J., et al., *Glycine administration attenuates skeletal muscle wasting in a mouse model of cancer cachexia.* Clin Nutr, 2014. **33**(3): p. 448-58.

91.	Batista, M.L., Jr., et al., *Heterogeneous time-dependent response of adipose tissue during the development of cancer cachexia.* J Endocrinol, 2012. **215**(3): p. 363-73.

92.	Li, Y.P. and M.B. Reid, *Effect of tumor necrosis factor-alpha on skeletal muscle metabolism.* Curr Opin Rheumatol, 2001. **13**(6): p. 483-7.

93.   Thoma, A. and A.P. Lightfoot, *NF-kB and Inflammatory Cytokine Signalling: Role in Skeletal Muscle Atrophy.* Adv Exp Med Biol, 2018. **1088**: p. 267-279.

94.   Zimmers, T.A., M.L. Fishel, and A. Bonetto, *STAT3 in the systemic inflammation of cancer cachexia.* Semin Cell Dev Biol, 2016. **54**: p. 28-41.

95.   Guadagnin, E., D. Mazala, and Y.W. Chen, *STAT3 in Skeletal Muscle Function and Disorders.* Int J Mol Sci, 2018. **19**(8).

96.   Brugarolas, J., et al., *Regulation of mTOR function in response to hypoxia by REDD1 and the TSC1/TSC2 tumor suppressor complex.* Genes Dev, 2004. **18**(23): p. 2893-904.

97.   Britto, F.A., et al., *Is REDD1 a metabolic double agent? Lessons from physiology and pathology.* Am J Physiol Cell Physiol, 2020. **319**(5): p. C807-C824.

98.   Gordon, B.S., et al., *Emerging role for regulated in development and DNA damage 1 (REDD1) in the regulation of skeletal muscle metabolism.* Am J Physiol Endocrinol Metab, 2016. **311**(1): p. E157-74.

99.   Puppa, M.J., et al., *Skeletal muscle glycoprotein 130's role in Lewis lung carcinoma-induced cachexia.* FASEB J, 2014. **28**(2): p. 998-1009.

100.   Arthur, S.T. and I.D. Cooley, *The effect of physiological stimuli on sarcopenia; impact of Notch and Wnt signaling on impaired aged skeletal muscle repair.* Int J Biol Sci, 2012. **8**(5): p. 731-60.

101.   Schroeter, E.H., J.A. Kisslinger, and R. Kopan, *Notch-1 signalling requires ligand-induced proteolytic release of intracellular domain.* Nature, 1998. **393**(6683): p. 382-6.

102.   Capaccione, K.M. and S.R. Pine, *The Notch signaling pathway as a mediator of tumor survival.* Carcinogenesis, 2013. **34**(7): p. 1420-30.

103.   Pine, S.R., *Rethinking Gamma-secretase Inhibitors for Treatment of Non-small-Cell Lung Cancer: Is Notch the Target?* Clin Cancer Res, 2018. **24**(24): p. 6136-6141.

104.   Sharif, A., et al., *Notch Transduction in Non-Small Cell Lung Cancer.* Int J Mol Sci, 2020. **21**(16).

105.   Guo, Q., et al., *Metformin inhibits growth of human non-small cell lung cancer cells via liver kinase B-1-independent activation of adenosine monophosphate-activated protein kinase.* Mol Med Rep, 2016. **13**(3): p. 2590-6.

106.   Storozhuk, Y., et al., *Metformin inhibits growth and enhances radiation response of non-small cell lung cancer (NSCLC) through ATM and AMPK.* Br J Cancer, 2013. **108**(10): p. 2021-32.

107.   Abbastabar, M., et al., *Multiple functions of p27 in cell cycle, apoptosis, epigenetic modification and transcriptional regulation for the control of cell growth: A double-edged sword protein.* DNA Repair (Amst), 2018. **69**: p. 63-72.

108.   Chu, I.M., L. Hengst, and J.M. Slingerland, *The Cdk inhibitor p27 in human cancer: prognostic potential and relevance to anticancer therapy.* Nat Rev Cancer, 2008. **8**(4): p. 253-67.

109.   Abbas, T. and A. Dutta, *p21 in cancer: intricate networks and multiple activities.* Nat Rev Cancer, 2009. **9**(6): p. 400-14.

110.   Hamilton, E. and J.R. Infante, *Targeting CDK4/6 in patients with cancer.* Cancer Treat Rev, 2016. **45**: p. 129-38.

111.   Wang, Y., et al., *Metformin inhibits lung cancer cells proliferation through repressing microRNA-222.* Biotechnol Lett, 2013. **35**(12): p. 2013-9.

112.   Lengyel, E., et al., *Metformin inhibits ovarian cancer growth and increases sensitivity to paclitaxel in mouse models.* Am J Obstet Gynecol, 2015. **212**(4): p. 479 e1-479 e10.

113.   Yang, B., et al., *Metformin depresses overactivated Notch1/Hes1 signaling in colorectal cancer patients with type 2 diabetes mellitus.* Anticancer Drugs, 2017. **28**(5): p. 531-539.

114.   Tendler, S., et al., *The prognostic implications of Notch1, Hes1, Ascl1, and DLL3 protein expression in SCLC patients receiving platinum-based chemotherapy.* PLoS One, 2020. **15**(10): p. e0240973.

115.   Rani, A., et al., *HES1 in immunity and cancer.* Cytokine Growth Factor Rev, 2016. **30**: p. 113-7.

116.   Cao, N., et al., *Metformin Synergistically Enhanced the Antitumor Activity of Celecoxib in Human Non-Small Cell Lung Cancer Cells.* Front Pharmacol, 2020. **11**: p. 1094.

117. Jin, H.O., et al., *Redd1 inhibits the invasiveness of non-small cell lung cancer cells.* Biochem Biophys Res Commun, 2011. **407**(3): p. 507-11.

118. Morelli, A.P., et al., *Metformin impairs cisplatin resistance effects in A549 lung cancer cells through mTOR signaling and other metabolic pathways.* Int J Oncol, 2021. **58**(6).

119. Yu, H., D. Pardoll, and R. Jove, *STATs in cancer inflammation and immunity: a leading role for STAT3.* Nature Reviews Cancer, 2009. **9**(11): p. 798-809.

120. Lin, C.C., et al., *Metformin enhances cisplatin cytotoxicity by suppressing signal transducer and activator of transcription-3 activity independently of the liver kinase B1-AMP-activated protein kinase pathway.* Am J Respir Cell Mol Biol, 2013. **49**(2): p. 241-50.

121. Deng, X.S., et al., *Metformin targets Stat3 to inhibit cell growth and induce apoptosis in triple-negative breast cancers.* Cell Cycle, 2012. **11**(2): p. 367-76.

122. Tan, X.L., et al., *Metformin suppresses pancreatic tumor growth with inhibition of NFκB/STAT3 inflammatory signaling.* Pancreas, 2015. **44**(4): p. 636-47.

123. Li, L.T., et al., *Ki67 is a promising molecular target in the diagnosis of cancer (review).* Mol Med Rep, 2015. **11**(3): p. 1566-72.

124. McCreight, L.J., C.J. Bailey, and E.R. Pearson, *Metformin and the gastrointestinal tract.* Diabetologia, 2016. **59**(3): p. 426-35.

125. Viollet, B., et al., *Cellular and molecular mechanisms of metformin: an overview.* Clin Sci (Lond), 2012. **122**(6): p. 253-70.

126. Graham, G.G., et al., *Clinical pharmacokinetics of metformin.* Clin Pharmacokinet, 2011. **50**(2): p. 81-98.

127. Zhang, H.H. and X.L. Guo, *Combinational strategies of metformin and chemotherapy in cancers.* Cancer Chemother Pharmacol, 2016. **78**(1): p. 13-26.

APPENDIX 1: INSTITUTIONAL ANIMAL CARE AND USE COMMITTEE APPROVAL
LETTER

UNC CHARLOTTE

Research and Economic Development

Office of Research Compliance

9201 University City Boulevard, Charlotte, NC 28223-0001
t/ 704.687.1876 | f/ 704.687.0980 | http://research.uncc.edu/compliance-ethics

Notice of Initial Protocol Approval

To:	**Dr. Joseph Marino** **Department of Kinesiology**
From:	**Dr. Yvette Huet** **IACUC Chair**
Subject:	**Approval of Protocol**
Protocol #:	**18-005**
Title:	**Tracking Lewis Lung Carcinoma Tumor Growth with the IVIS: A Pilot Study**
Approval Date:	**07/29/2018**

The Institutional Animal Care and Use Committee (IACUC) approved the protocol entitled **"Tracking Lewis Lung Carcinoma Tumor Growth with the IVIS: A Pilot Study."** Approvals are valid for one year and may be renewed before the anniversary of the original approval date for a total of three years. After three years, a new protocol application must be submitted to continue the study. Please note the following information:

Initial Approval date:	**07/29/2018**
Renewal 1 – due and approved before:	07/29/2019
Renewal 2 – due and approved before:	07/29/2020
Expiration date:	07/29/2021

Please note that it is the investigator's responsibility to promptly inform the committee of any changes in the proposed research, as well as any unanticipated problems that may occur involving care and use of animals. All changes (e.g. personnel additions, change in animal strain, change in procedures, etc.) must be submitted to the IACUC via an Amendment. All forms (e.g. amendments, annual renewal, etc.) can be found at:
http://research.uncc.edu/departments/office-research-compliance-orc/animal-care-use/protocol-application-forms

Before starting any protocol involving survival surgery, tumor and/or disease induction, and any other painful animal procedure, a meeting with the Attending Veterinarian, Vivarium Director, and Vivarium staff is required. If the research involves surgical procedures, it is also the investigator's responsibility to maintain detailed surgical records. These records must be approved by the Vivarium Director and the Attending Veterinarian and a copy must be kept with the animals at all times.

To better help you and your research team, please inform Vivarium personnel which phase/specific aim of your protocol is being conducted at any given time. It is helpful for the staff to know which endpoints are required for the phase/specific aim being investigated.

NOTE: **Since a pilot study is being proposed, per IACUC policy, a progress report will be due to the IACUC approximately 90 days from the date of initiation of this study, or by October 30, 2018.**

A renewal/status report is due annually for IACUC protocols. The annual renewal application can be accessed via the above-listed website. If you do not plan to continue your study at the time of your renewal anniversary date, please contact the Office of Research Compliance before the anniversary date to terminate your study.

If you need additional assistance, please contact Cindy Stone in the Office of Research Compliance at (704) 687-1872 or via email at C.Stone@uncc.edu.

The UNIVERSITY *of* NORTH CAROLINA *at* CHARLOTTE
An Equal Opportunity/Affirmative Action Employer

APPENDIX 2: INSTITUTIONAL BIOSAFETY APPROVAL LETTER

UNC CHARLOTTE
Research and Economic Development
Office of Research Compliance
9201 University City Blvd., Charlotte, NC 28223
t/ 704.687.1825 | f/ 704.687.0980 | http://research.uncc.edu/compliance-ethics

Institutional Biosafety Committee (IBC)

Certificate of Approval and Registration for BSL-1 work

To:	Dr. Joseph Marino
	Department of Kinesiology
From:	Dr. Angelica N. Martins – Biosafety Officer
Protocol Title:	"Tracking Lewis Lung Carcinoma tumor growth with the IVIS: A Pilot Study"
IBC Protocol #:	18-991
Agent/s and Material/s Declared:	Vertebrate animal work and mice cell line.
BSL/Risk Group Classification:	BSL-1
Approval Date:	July 30, 2018.

The Institutional Biosafety Committee (IBC) has reviewed your APPROVED your Biosafety Protocol. The IBC concurs with your classification and the stated precautions for using these agent(s) or material(s). Approvals are valid for five years and should be renewed before the fifth anniversary of the original approval date. After five years, a new protocol application must be approved to continue the study. Your protocol will reach 5-year expiration on **July 29, 2023.**

It is the investigator's responsibility to inform the IBC of any changes in the proposed research (e.g. agents and materials used, location of agents, type of manipulations, etc.); the investigator must inform the IBC of these changes via an amended protocol. Personnel changes should be informed to the BSO through email.
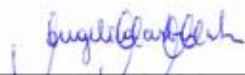
Also, the investigator is responsible for ensuring the following:

1. Laboratory personnel wears lab coats, disposable gloves, and any additional Personal Protective Equipment (PPE) required by the IBC.
2. Laboratory personnel must wash their hands after working with potentially hazardous materials and before leaving the laboratory.
3. Eating, drinking, smoking, handling contact lenses, applying cosmetics, and storing food for human consumption must not be permitted in laboratory areas. Food must be stored outside the laboratory area in cabinets or refrigerators designated and used for this purpose.

4. The laboratory supervisor must ensure that laboratory personnel receives appropriate training regarding their duties, the necessary precautions to prevent exposures and exposure evaluation procedures.

If you have any questions, please contact Dr. Angelica N. Martins in the Office of Research Compliance at 704-687-1825.

_____   August 16, 2018

Angelica N. Martins, PhD, RBP   _____
Biosafety Officer   Date
Office of Research Compliance